1989 - 1995: A Galileo NAVIGATION SPACE ODYSSEY ORBIT DETERMINATION

R.J. HAW, P.G. ANTREASIAN, E.J. GRAAT, T.P. McELRATH, F.T. NICHOLSON
Navigation and Flight Mechanics, Jet Propulsion Laboratory, Pasadena California USA 91109
Internet (first author): rjh@charybdis.jpl.nasa.gov

The Galileo spacecraft reached Jupiter on December 8, 1995. During its six year voyage Galileo encountered six celestial bodies. Accurate determinations of the spacecraft's orbit prior to passing these bodies played a critical role in successfully delivering Galileo to Jupiter, and for yielding new findings. The navigation of Galileo past each of these bodies is discussed and illustrated, and the spacecraft's discoveries at each encounter summarized.

---

1. INTRODUCTION

On December 7, 1995 the Galileo spacecraft came within 900 kilometers of the volcanoes of Jupiter's satellite Io, and less than five hours later was in a position to receive the unprecedented first-ever signal from an atmosphere-sampling probe falling into Jupiter's clouds below. After two more hours the spacecraft executed an on-board command sequence causing the spaceraft's retropropulsion module to thrust for 48 minutes, subtracting the velocity necessary to place Galileo into an elliptical orbit around Jupiter. These three remarkable feats -- the first near passage of a spacecraft with a satellite of Jupiter, the first *in situ* measurements of an outer planet's atmosphere, and the first spacecraft to orbit an outer planet -- were only the latest in a six year voyage traversing a length of 25 A.U. (90% the Earth-Neptune distance). This review will describe highlights of the determination of Galileo's orbit and some of its scientific discoveries during this six year period, from launch through arrival at Jupiter.

2. MISSION OVERVIEW

Galileo departed Earth bound for Jupiter on October 18, 1989. The mission's objective was and is, to undertake an intensive scientific investigation of Jupiter's atmosphere, satellites, and magnetosphere and to investigate targets

of opportunity encountered enroute. As configured at launch, the Galileo spacecraft consisted of a probe vehicle to penetrate deep into Jupiter's atmosphere and an orbiter vehicle to deliver the probe and to perform scientific observations of the Jupiter system from orbit.

Prior circumstances prevented Galileo from following a direct path to Jupiter [1], and mission designers were obliged to find an alternate trajectory for the mission. The Earth-to-Jupiter interplanetary trajectory eventually selected first took Galileo past Venus and Earth as shown in figs. 1, 2, and 3. Fig. 1 represents Galileo's first orbit around the Sun. Similarly, fig. 2 depicts the spacecraft's second revolution of the Sun, while the last lap to Jupiter is shown in fig. 3. This particular trajectory harnesses the gravity of one planet to deflect the spacecraft on towards another. The accelerations from nearby planets will cause spacecraft to deviate from their approach asymptote and the resultant bending, by redirecting the spacecraft velocity in heliocentric space, behaves like a deflection. In the process, the spacecraft's heliocentric speed can also change and by carefully managing such speed changes, the magnitude of Galileo's velocity was increased until sufficient energy for passage to Jupiter was attained. This 'gravity-assist' technique minimizes spacecraft propellant consumption and offers, as in the case of Galileo, often the only practical method of reaching the destination.

NOTE: fig. 1. Galileo Trajectory: Launch to Earth-1 Encounter **IN BACK OF DOCUMENT**

NOTE: fig. 2. Galileo Trajectory: Earth-1 to Earth-2 Encounter **IN BACK OF DOCUMENT**

NOTE: fig. 3. Galileo Trajectory: Launch to Jupiter Encounter **IN BACK OF DOCUMENT**

The governing conic equation for a gravity-assist deflection is:

$$\sin \alpha/2 = (1 + R_p v_\infty^2 / \mu)^{-1} \qquad (1)$$

where α is the deflection angle between the inbound and outbound asymptotes, R_p is pericenter radius, v_∞ is the hyperbolic excess velocity of the spacecraft and μ is the gravitational constant of the target body.

The flyby of Venus in February 1990, shown in fig. 1, supplied a gravity-assist to Galileo and was followed by a similar assist at Earth ten months later. An encounter with the asteroid Gaspra occurred in October 1991 (fig. 2), but the mass of that body was too slight to effect a gravity-assist. That flyby, however, provided the first-ever close-up observations of a main belt asteroid. A second Earth gravity-assist occurred in December 1992. Fig. 3 illustrates the final portion of the trip to Jupiter. Midway along that leg, in August 1993, Galileo successfully rendezvoused

with the asteroid Ida. The results of that encounter included the discovery of Dactyl, the first natural satellite of an asteroid ever observed.

In October 1993, about five weeks after the Ida encounter, spacecraft thrusters redirected Galileo from its post-Ida trajectory toward Jupiter. Since the probe had no onboard propulsion system, the orbiter/probe spacecraft was placed on a trajectory such that, once released, the probe would fall ballistically into the desired Jupiter aimpoint (defined at an altitude of 450 km above the reference Jupiter oblate spheroid). Two subsequent small trajectory correction maneuvers (TCMs) performed in February 1994 and April 1995 removed small errors in the probe entry conditions prior to probe release.

In July 1994 the spacecraft's unique position in the solar system placed it at a phase angle with respect to Jupiter that fortuitously enabled Galileo to observe the comet Shoemaker-Levy collision with Jupiter. Galileo thus became the sole observer to directly record those events, not just the residual plumes and scars [2].

On July 13, 1995, the probe separated successfully from the orbiter. Five months later the probe entered Jupiter's atmosphere on December 7 1995, at 22:04:44 UTC ± 3.1 seconds -- 18 seconds later than planned but well within the 3 minute error bars bounding the target entry time. *A posteriori* analysis of probe results showed more helium in Jupiter than was anticipated and more extreme environmental conditions. Temperatures exceeded the expected ranges and water vapor was less abundant than believed [3].

Two weeks after probe release, on July 27, a maneuver deflected the orbiter from its Jupiter impact trajectory onto a path designed to fly by Io on December 7 at an altitude of 1000 km, and subsequently to overfly the probe during its descent. Four additional maneuvers were scheduled between the deflection maneuver and the Io flyby in order to refine the inbound trajectory. Only the first of those maneuvers occurred (in late August). The project team elected not to perform additional maneuvers since concern was considerable for maintaining the spacecraft in a stable, healthy state and the fuel penalty was not costly.

The Io encounter occurred about four hours before Jupiter closest approach. The Io flyby, yet another gravity-assist, this time slowed the spacecraft by 175 ms^{-1} or 20% of the necessary velocity reduction needed to enter Jupiter orbit. About seven hours after the Io encounter the main engine burn slowed the spacecraft by an additional 645 ms^{-1}. The data returned from the spacecraft during these events revealed later the true Io flyby altitude to be 897 km*, the

* A consequence of electing not to perform additional Io approach maneuvers. See Section 4.

Jupiter closest approach altitude to be 214,573 km (3 Jupiter radii) and main engine performance to be within a commendable 0.14% of its design thrust. Galileo was now in orbit around Jupiter. The spacecraft had launched with 934 kg of propellant and 291 kg remained, an ample reserve to conduct the remainder of the mission.

3. ELEMENTS OF INTERPLANETARY NAVIGATION

Navigation means the skill in plotting a route and directing a craft along it. Since the principle forces acting on a spacecraft apart from its thrusters are gravitational, knowing a spacecraft's position and velocity at a particular time permits a unique trajectory to be computed. In practise, navigators determine spacecraft position and velocity (state), calculate whether the spacecraft will reach its goal on time, and steer it back on course with thrusters if necessary. The angle α in equation (1) depends upon position and velocity, so gravity-assist trajectories require precise spacecraft navigation along the inbound asymptote to minimize a potentially large post-encounter thrusting maneuver (necessary to correct flyby errors).

As a discipline, interplanetary navigation consists of constrained optimization and adaptive parameter estimation. Detailed parameter estimates (*e.g.* spacecraft state) must be computed from measurements. This process, of determining spacecraft trajectories from observations, is termed orbit determination. The limiting accuracy of this process depends on the time span of the observations, the geometric characteristics of the trajectory and the accuracy of the dynamical and observational models. In general, trajectory knowledge is poor at the beginning and improves slowly over months of observations (or tracking). Improvement is manifested via modest changes to spacecraft state and the other parameters comprising the dynamical and observational models and by reductions in the uncertainties associated with those parameters. In the end, the process yields not a single estimated trajectory but a corridor in state space. A calculation can then assign a probability to the spacecraft's location at any one time. In this way uncertainties in Galileo's current state are transformed into future uncertainties at the target body.

Uncertainties at the target body may be visualized in probability space as an ellipse placed in a plane perpendicular to the incoming trajectory, at the point of closest approach. This plane is called a Bplane (for historical reasons) and an illustration of the coordinate system is provided in fig. 4. The radius from the center of the target planet to the point the incoming asymptote intersects the Bplane is called the impact parameter, **B**. The

elliptical area represents an uncertainty dispersion and is one measure of the statistical uncertainty in the predicted path of the spacecraft.

NOTE: fig. 4. Geometry of the Bplane **IN BACK OF DOCUMENT**

Near the beginning of a trajectory, far from the target, velocity errors are the chief source of Bplane error and the dispersions are large. As more data is acquired, velocity errors become less significant and the dispersions shrink until the effects of small un-modelled forces on the spacecraft begin to cancel information gained from the additional tracking. Maneuver thrusting introduces new errors which increase dispersions. The target dispersion consisting of all uncertainties, including both orbit determination and expected maneuver errors, is a pre-maneuver estimate of all likely future trajectories the spacecraft might follow.

Two basic measurements are utilized in orbit determination: radiometric and optical. Radiometric data are obtained by analyzing radio signals from the spacecraft and optical data are obtained from the spacecraft's camera. We will briefly consider these data types below, so that their importance to Galileo may be understood. Prior to that discussion, however, we wish to discuss a specific component failure in the Galileo telecommunication subsystem.

A spacecraft's telecommunication subsystem links it to Earth and Galileo was designed to communicate through a 4.8 meter diameter high gain antenna using a carrier frequency of 8.4 Ghz. The antenna, designed to open like an umbrella, only partially deployed when commanded to open in April 1991. Since that time all efforts to free the stuck antenna have failed. As a result, all transmissions from the spacecraft have occurred over a backup low gain antenna (diameter $\approx$ 0.1 meter), using a carrier frequency of 2.3 Ghz. The spacecraft transmitter radiates a sufficient 20 watts, but since the low gain antenna performance near-axis is approximately 40 dB lower than the directional high gain antenna, a maximum of approximately 20 to 30 bits s^{-1} can be received at any single ground station (a rate only slightly greater than manual transmission of morse code). This configuration has considerably restricted the acquisition of navigation, as well as science data. Yet despite this significant degradation in data quantity (and quality), the navigation process has been modified to substantially and so far successfully, counter the low gain antenna limitations.

3.1 RADIO MEASUREMENTS

Radiometric data obtained by the radio subsystem falls into one of three classifications: range, range-rate, and simultaneous one-way range. The range measurement functions by determining round-trip travel time of the radio signal. Since the speed of light is known precisely, this yields the distance to the spacecraft. In theory, the limiting accuracy for Galileo's ranging system is approximately 10 nanoseconds, or about 1 meter in distance from Earth. This theoretical limit is unachievable in practise, for several reasons. The positions on Earth of the ground station antennas are not known to better than about 1 meter accuracy, and environmental conditions (*e.g.* space plasmas) can contribute to significant degradation of the measurement.[†] Moreover, point-to-point accuracy of the measurement depends on signal strength. Thus as range increases, the measurement becomes increasingly difficult to acquire. These reasons and a general philosophy of conservatism, contributed to assigning *a priori* in-flight range measurement accuracies of 100 m to 1 km to the Galileo data. After incorporating these data into a solution and adjusting the trajectory to better fit the data, the observed scatter in the data exhibited root mean square measurement uncertainties of 3 m to 70 m (*a posteriori*). This increase in accuracy from the *a priori* to the *a posteriori* condition demonstrates two points. First, that the data along some parts of the trajectory was very good (near its limiting accuracy) and second, that the one to two order-of-magnitude improvement in measurement accuracy adjudicated the cogency of range data to the solution. In time, the distance from Earth to Galileo precluded acquisition of further ranging measurements (at a range of about 3 A.U., or near the orbit of Ida).

Range-rate, or doppler, measurements utilize the doppler shift in the frequency of a received radio signal caused by the relative motion of the transmitter and receiver. This measurement yields information on the radial component of the spacecraft's velocity. The doppler relation can be expressed as:

$$f = f_o \sqrt{(1 - v^2/c^2)}(1 - v/c \cos\alpha)^{-1} \qquad (2)$$

where f is the measured observable in Hz, f_o is the reference frequency of the source without relative motion, v is the source velocity, c is the speed of light, and α is the angle between the velocity of the source and the line-of-sight from source to receiver. Since the spacecraft communicates over a narrow frequency range, a shift in frequency can be equivalently stated as a change in velocity (15.3 Hz $\equiv$ 1 m s^{-1}).

The limiting accuracy for doppler measurements is about 0.1 mm s^{-1} (a measurement that in practise is obtained by essentially determining the change in range to the spacecraft over a finite period). Ideal signal conditions seldom

[†] The error caused by propagation through plasma is inversely proportional to square of the signal's carrier frequency.

exist, however, and just as for ranging errors can be induced by media (specifically the terrestrial ionosphere and troposphere, and solar plasma). These errors may be reduced but not wholly eliminated by calibrating the data with external information. In practise, a data accuracy of 1 mm s^{-1} is considered standard, although values as low as 0.5 mm s^{-1} are often observed.

One problem associated with range-rate is weakness in readily determining angular positions on the celestial sphere, with a characteristic tracking error at standard accuracies of about 250 nanoradians (positional accuracy of 150 km at Jupiter). Range-rate uses a time history to improve angular measurements, so long spans of doppler data (at least several months) can substantially reduce this error. Even long data spans, however, cannot remove the singularity which occurs at low declinations (within about ±15° of the celestial equator). The source of this trouble can be seen by expressing the range-rate of a distant spacecraft in terms of the geometry of the observation. The range-rate relation is [4]:

$$d\rho/dt \approx dr/dt + \omega r_s \cos\theta \sin(\omega t + \phi)$$

which reduces to:

$$\Delta\theta \sim (\sin\theta)^{-1} \tag{3}$$

where $d\rho/dt$ is the range-rate observable, r is the geocentric spacecraft range, r_s is the distance of the observer from the Earth's spin axis, ω is Earth's rotation rate, θ and ϕ are the spacecraft's declination and right ascension, respectively. The ability to determine spacecraft declination, therefore, is inversely related to the sine of the geocentric declination. At low declinations, the measurement degrades appreciably.

The third data type, simultaneous one-way ranging, can remove much of this indeterminancy in low elevation observations. Simultaneous ranging measurements depend on a pair of widely separated ground tracking stations. The measurement is interferometric: one-way range data received nearly simultaneously at the two ground stations is differenced with a signal from a reference extragalactic radio source (*e.g.* quasar). The observable computed from this difference of differenced-one-way-range (known as ΔDOR) is a time delay (or distance -- obtained by multiplying the time delay by the speed of light. See fig. 5.) Note that this observable is not a ranging measurement; ΔDOR complements range by measuring displacements in the celestial sphere (perpendicular to the line-of-sight from Earth), a component not readily visible with the other radio data types. From the equation in fig. 5, it can be shown that ΔDOR measurements respond at low declinations in the following way:

$$\Delta\theta \sim (\cos\theta)^{-1} \quad (4)$$

Thus ΔDOR does not suffer the low declination limitation of doppler.

NOTE: fig. 5. Geometry for ΔDOR Observations **IN BACK OF DOCUMENT**

In theory, an angular uncertainty of about 20 nanoradians is possible with Galileo ΔDOR observations (equivalent to a positional accuracy at Jupiter of about 15 km). For comparison, non-interferometric measurements from a single antenna are limited to an angular uncertainty on the order of 1 milliradian, or 50,000 km. In actual practise, ΔDOR uncertainties of 30 to 100 nanoradians (over distances of a fraction of an A.U. to 3 A.U.) have been observed by Galileo. The larger uncertainties were associated with more distant transmissions.

These three radiometric data types in combination form a complementary measurement triad, a powerful sensory system that provides significantly greater insight into spacecraft behavior than would be possible with only a single data type. In practise, however, the preponderance of Galileo tracking data has consisted of doppler measurements. Ranging data, limited by the present condition of Galileo's telecommunication subsystem, were available only within the inner solar system. Interferometric measurements require additional (although not unreasonable) resources and for this reason have been used sparingly.

3.2 OPTICAL MEASUREMENTS

Optical data augment radiometric data by directly determining the spacecraft's position in relation to the target of interest, say an asteroid, rather than with respect to Earth. The technique also determines (or improves) the natural orbit of the observed asteroid. Such information is invaluable when the *a priori* ephemeris has uncertainties too large for navigation or imaging. To be specific, capturing a high resolution image of a 50 km asteroid when its location is not known to better than 500 km would exceed the resources of Galileo.

Optical navigation observations consist of on-board camera recordings of say, an asteroid and background stars, imaged when the spacecraft is far from the asteroid (millions of kilometers). Analogous to a ΔDOR measurement, knowing the positions of reference stars fixes the angular position of the center of the target body.

The instrument used to acquire these images consists of a single 150 cm Cassegrain f/8.5 telescope joined to an 800x800 element CCD sensor array. The field of view is 0.47°. Measurements are accurate to one second of arc

(one-half CCD pixel, or about 5000 nanoradians). This accuracy provides orbits good to about 1 km for every 200,000 km distance from the target body -- entirely adequate since the spacecraft is so much closer to its target than to Earth.

4. GALILEO INTERPLANETARY NAVIGATION

In this section we summarize graphically the salient navigation events for Galileo during its six year voyage. The circumstances leading up to each encounter are detailed and alternate trajectories compared. The uncertainty dispersion associated with each trajectory in the figures that follow represents a prediction with a probability of 67% that the actual trajectory error at the target will fall within those bounds. Sometimes an orbit solution violated this prediction and for those cases an explanation is provided.

Inbound to an encounter, the navigation subsystem knows spacecraft state to some level of certainty. (Sufficient accuracy also assures success of the planned observations.) After the encounter, post-encounter studies or reconstructions can determine the true closest approach point of the spacecraft to high accuracy. In turn these reconstructions may be compared against the predicted target accuracies.

4.1 VENUS ENCOUNTER

Galileo was delivered to Earth orbit on October 18, 1989 aboard the Space Shuttle *Atlantis*. The Inertial Upper Stage booster deployed along with Galileo provided the interplanetary injection eight hours after attaining Earth orbit. This booster, unable to supply sufficient energy to increase Galileo's velocity by the 9 km s^{-1} necessary to reach Jupiter directly, instead subtracted 3.9 km s^{-1} from the orbital speed of Galileo, allowing the spacecraft to fall inward to Venus. The initial aimpoint was biased from the final Venus target to eliminate any risk of a booster collision with Venus. The biased target, shown in fig. 6, is labelled 'Injection target' (in a Venus-centered, Earth Mean Ecliptic (EMO) of 1950 coordinate system). The path imparted to Galileo was expected to place it (in a statistical sense) two out of three times within the indicated ellipse. Indeed, after five days of post-injection tracking, the orbit determined for Galileo indicated that the booster had performed exemplarly. This solution is denoted 'Injection achieved' in fig. 6.

NOTE: fig. 6. Venus Encounter Dispersions (67% certainty) Venus-centered Earth Mean Ecliptic (1950) **IN BACK OF DOCUMENT**

The velocity adjustment required to steer Galileo from its injection trajectory to Venus is indicated in fig. 6 as TCM1, the first trajectory correction maneuver. This foremost maneuver executed on November 9 with a magnitude of 16 m s^{-1}. One additional maneuver six weeks later corrected the residual velocity errors in TCM1. The second maneuver placed Galileo on a trajectory sufficiently close to the target such that another planned Venus approach maneuver was cancelled.

Uncertainties in the Venus trajectory two weeks from encounter are illustrated at the bottom of fig. 6. The trajectory estimate and the target both lay inside the error bounds of the solution, indicating that the trajectory was likely to miss the aimpoint by 13 km ± 15 (with a probability of 67%), passing beneath the target. The reconstruction shows that the actual trajectory was far closer to the target than predicted -- missing by just 5 km – but fell much higher in the Bplane than expected (a possible but not probable occurence). This inconsistent result was traced later to misaligned attitude adjustment thrusters and mismodelled solar pressure forces (the cross-sectional area reported by the spacecraft builders was found to be in error by 20%).

Galileo's flyby of Venus occurred at an altitude of 16,123 km on February 10, 1990. The resulting gravity-assist increased the spacecraft's heliocentric velocity by 2.2 km s^{-1}.

4.2 EARTH ENCOUNTER (1990)

Earth encounter navigation followed a strategy designed to rigorously minimize the risk of collision with Earth. The implementation called for a biased initial aimpoint, followed by successive updated aimpoints each lying in turn closer to the final target [5]. Fig. 7 shows this effect in the Bplane for the first Earth encounter (in an Earth-centered, EMO of 1950 coordinate system). Each maneuver aimpoint was the closest point to the final target consistent with a probability of impacting the Earth of 10^{-6}. The Earth-1 target lay at an altitude of 952 km, a point targetted by the final two pre-Earth maneuvers, TCM7 and TCM8.

NOTE: fig. 7. Earth-1 Encounter Dispersions (67% certainty), Earth Mean Ecliptic (1950)**IN BACK OF DOCUMENT**

Navigation of the Venus encounter had utilized doppler and range data. The Earth-1 approach employed those data types, as well as ΔDOR. Fig. 8 illustrates the capability of ΔDOR. This fig. represents the situation when the spacecraft was 40 days distant from Earth, at a declination of 13.7°.

The doppler-only solution in fig. 8 had large B·R uncertainties associated with it, representing the degraded resolution of doppler data along the declination component (declination roughly equates to the B·R coordinate, and right ascension to B·T). Adding range data reduced uncertainty in B·T, but the B·R uncertainty remained relatively unchanged since both doppler and range provide information only along the Earth-line. The third ellipse shows that the dispersions for a solution with all three radio data types (including ΔDOR) significantly reduced B·R uncertainty. This latter solution also lies closest to the reconstruction performed after the flyby. All three solutions remained statistically consistent with each other.

NOTE: fig. 8 Earth Encounter Dispersions on Oct. 30 1990 (67% certainty) **IN BACK OF DOCUMENT**
Earth Mean Ecliptic (1950)

As the spacecraft approached Earth, knowledge of its orbit improved. Fig. 7 shows the orbit determination uncertainties 15 days prior to arrival. The final pre-Earth maneuver was designed at this time to correct a 60 km altitude error. After the flyby, reconstruction placed the spacecraft 0.4 seconds late in time of closest approach (arriving at 20:34:34.4 UTC on December 8, 1990), 960 km above the northeast Caribbean Sea (8 km high, with respect to the target). The reconstruction is consistent (just barely) with the prediction 15 days earlier.

Outbound asymptotes are sensitive to flyby altitude, and this sensitivity has a cost associated with it. The cost is shown in the mission propellant cost contour plot in fig. 7. Cost contours are useful for estimating future costs as a function of two dimensional Bplane errors. At the center of the cost contour is the optimal Earth-1 gravity-assist aimpoint. This is the point through which an ideal trajectory would pass. In practical situations it is unlikely a real mission will achieve this precision, and the contours in fig. 7 measure the propellant cost (in meters per second) of redirecting the spacecraft back to the optimal trajectory for a specified miss-vector in the Bplane. The miss shown in fig. 7 resulted in a cost of approximately 7.6 m s^{-1} (without the final altitude correction, the miss would have cost 41 m s^{-1}).

The Earth gravity-assist added 5.2 km s^{-1} to the spacecraft's heliocentric velocity. The error incurred at the flyby was corrected by two discrete maneuvers within three months of the encounter.

The ΔDOR campaign for the Earth-1 encounter was undertaken for the singular purpose of achieving a highly accurate delivery in order to conserve propellant. The actual savings was only one-half the expected quantity. The likely cause of this shortfall was an inadequately modelled error source. The size of the orbit determination

dispersion in fig. 7 is smaller than the delivery dispersion for TCM8, a behavior suggesting that the preceding maneuver was mismodelled. However, ΔDOR's high fidelity measurement was supposed to prevent this kind of acceleration mismodelling, so the lack of fidelity is surprising. The root of the mismodelling can be traced to the ΔDOR data set. A majority of the pre-TCM7 ΔDOR observations either failed or were cancelled, thereby reducing the time span of the pre-TCM7 observations and marginalizing visibility into spacecraft performance.

4.3 GASPRA ENCOUNTER

The Earth-1 gravity-assist flung Galileo outward into the asteroid belt, where it accomplished the first-ever encounter with a main-belt asteroid, asteroid 951 Gaspra, on October 29, 1991. In anticipation of this encounter, efforts were necessary to improve the knowledge of Gaspra's orbit, since the asteroid's *a priori* ephemeris was poorly known and as such could not support scientific observations.

Some characteristics of Gaspra are listed in Table 1.

TABLE 1: *Characteristics of 951 Gaspra*

Epoch	October 1, 1989
Perihelion distance	1.826 AU
Eccentricity	0.1737
Inclination to ecliptic	4.100 degrees
Orbital period	3.286 years
Rotation period	7 hours
Composition	stony

Table 2 lists uncertainties for the Gaspra *a priori* ephemeris as expected at the time of encounter. The values in Table 2 are given in a heliocentric RTN coordinate system, defined by a Sun-asteroid unit vector (**R**), a vector normal to **R** and normal to the asteroid's orbit plane (**N**), and by a vector (**T**), where **T** = **N** x **R**.

TABLE 2: *Gaspra Ephemeris Error (67% certainty)*

	A Priori	**Pre-encounter**	**Post-encounter Change from Pre-encounter**
R (km)	±258	±126	3 ± 102
T (km)	±826	±254	-77 ± 115
N (km)	±451	±155	23 ± 138
Encounter time (s)	±66	±32	6 ± 15

Ground-based observation efforts sought to improve the *a priori* ephemeris to a degree commensurate with the planned scientific objectives. Therefore a special observing campaign of Gaspra was conducted from 1989 to 1991 to

improve its ephemeris. The ephemeris uncertainties derived from the ground-based campaign are listed under Pre-encounter in the third column of Table 2. The estimated differences between the ground-based determination of Gaspra and where we now believe Gaspra was actually located at the time of the encounter, and the uncertainties in those offsets, are tabulated in the last column of Table 2 [6]. Fig. 9 illustrates these uncertainties graphically.

NOTE: fig. 9. Gaspra Ephemeris Error (67% certainty) **IN BACK OF DOCUMENT**

The path to Gaspra in the Bplane is illustrated in the upper half of fig. 10. This peculiar sequence of steps was the result of controlling the trajectory to satisfy Earth avoidance requirements at the second Earth encounter.

Optical navigation was employed for the first time at Gaspra. The post-encounter ephemeris uncertainties in the fourth column of Table 2 (and fig. 9) indicate the value of this data. Without optical images for guidance, the error in Gaspra's position would have gone uncorrected and at the time of closest approach, the pointing of the camera would have been in error by about five fields-of-view.

NOTE: fig. 10. Gaspra Encounter Dispersions (67% certainty) **IN BACK OF DOCUMENT**
Gaspra-centered Earth Mean Ecliptic (1950)

A total of four navigation images were acquired. The images were shuttered 53 days, 31 days, 16 days, and 8 days before the encounter, respectively. The range to Gaspra at the time of the first shuttering was $37 \cdot 10^6$ km, and for the last equalled $5.8 \cdot 10^6$ km. Fig. 11 reproduces these optical navigation images. The severely restricted downlink telemetry rate from the spacecraft forced a nonstandard technique called a "single-frame-mosaic" image. This technique maximized the probability of capturing Gaspra and multiple stars within a single picture, as well as allowing multiple optical measurements per frame. To achieve this result the camera's shutter was held open while moving the camera platform, thereby smearing or "trailing" the point sources within each image. In the first of the images shown here, boxes have been placed around loci on the "trails" to indicate the location of each measurement.

NOTE: fig. 11. Gaspra Single-Frame Mosaic Optical Navigation Images **IN BACK OF DOCUMENT**

Recalling fig. 10, the improvement in the orbit from successive images of Gaspra is evident in the lower half of that figure. As indicated in the figure, the solution without optical data was offset nearly 100 km from the true trajectory (the difference between the ground-based and spacecraft-based Gaspra ephemeris). Post-encounter reconstruction of the Gaspra flyby showed that the spacecraft passed 4 ± 10 km above the target altitude of 1600 km, and arrived 3 ± 10 seconds early, at 22:36:57.5 UTC. Thus orbit errors partially compensated for ephemeris errors;

Gaspra's location was incorrect by 6 seconds in time-of-flight, but the spacecraft missed its target by only one-half that magnitude.

An image of Gaspra is presented in fig. 12. For scale, the long axis shown in the photograph is approximately 18 km in length. This photograph was shuttered at a range of 16,000 km.

NOTE: fig. 12. Gaspra **IN BACK OF DOCUMENT**

4.4 EARTH ENCOUNTER (1992)

The second Earth encounter seems to parallel the first, falling as it did on the same day of the year. Apart from similar dates and planets, though, the two encounters had little in common. The second encounter occurred over the South Atlantic ocean at an altitude of 303 km. At this altitude atmospheric drag effects became important and therefore were added to the spacecraft dynamic model.

The approach to Earth is illustrated in fig. 13. A post-Gaspra maneuver, TCM14, targetted the spacecraft to the indicated aimpoint in fig. 13. The actual trajectory passed far outside the delivery dispersion -- an improbable event. The cause was discovered to be a timing error in the spacecraft's implementation of the maneuver (a mis-positioning of the thruster centroid about the spacecraft spin axis). The sizable magnitude of TCM14 (21 m s^{-1}) uncovered this fault. (Orbit determination uncertainties dominate small thrusting events, masking errors in the implementation of those maneuvers. Only for large maneuvers are thrusting errors readily visible.) Similar excursions had occurred with previous large maneuvers (*e.g.* TCM4B), but had not been recognized as such at the time.

NOTE: fig. 13. Earth-2 Encounter Dispersions (67% certainty) Earth Mean Ecliptic (1950) **IN BACK OF DOCUMENT**

Also shown in fig. 13 are the orbit determination predictions 15 days prior to encounter. A comparison at this time between a solution including ΔDOR in the data set, and one that did not, is also shown. Similar to the first Earth approach, adding ΔDOR greatly improved knowledge of the trajectory. Unlike Earth-1, the spacecraft was located higher on the celestial sphere and the overall improvement could be traced to greater insight into the preceding maneuver. Including ΔDOR removed much of the plane-of-sky uncertainty not resolved with the doppler and range observations.

Encounter reconstruction showed the spacecraft missed the target low by 0.7 km and early by 0.1 second, reaching the point of closest approach at 15:09:24.9 UTC on December 8, 1992. The drag on Galileo from passage

through the atmosphere slowed the spacecraft by 5.9 ± 0.1 mm s^{-1}. This perturbation was sufficiently large to be included in subsequent trajectory modelling.

Another first-time achievement for Galileo was the successful tracking of the spacecraft by NASA's Tracking and Data Relay Satellite System (TDRSS). Galileo's low perigee left a gap in the ground stations' tracking coverage of nearly two hours around closest approach. During that time, however, Galileo was within the field-of-view of the spare TDRSS satellite parked at 62° west longitude. It was configured to observe the Galileo carrier signal to obtain a continuous doppler arc throughout the encounter period. This tracking during the encounter represented the first time TDRSS had been employed to track a spacecraft on a hyperbolic orbit [ref].

The accurate positioning of Galileo at closest approach meant that the trajectory needed a correction of only 1 m s^{-1} to compensate for the flyby error (mission cost contour in fig. 13). This correction was subsequently combined with an Ida targetting maneuver -- leading to cancellation of a scheduled post-Earth-2 maneuver, TCM18. The Earth-2 gravity-assist increased the spacecraft's heliocentric speed by 3.7 km s^{-1} to a value of 39.0 km s^{-1}. Galileo now had sufficient energy to reach Jupiter.

4.5 IDA ENCOUNTER

Preparations for the Ida encounter on August 28, 1993 paralleled the Gaspra effort nearly two years earlier. A ground-based observational campaign was initiated to improve the *a priori* Ida ephemeris, and a sequence of five "single-frame mosaic" optical navigation shutterings were planned during the approach phase (only three were successful).

Some characteristics of Ida are listed in Table 3.

TABLE 3: *Characteristics of 243 Ida*

Epoch	November 9, 1993
Perihelion distance	2.73 AU
Eccentricity	0.0434
Inclination to ecliptic	1.131 degrees
Orbital period	4.84 years
Rotation period	4.6 hours
Composition	stony

Table 4 lists the uncertainties in Ida's ephemeris (under *A Priori*) that would have existed at the time of encounter if a directed ground-based observation campaign had not been undertaken. The Ida astrometric campaign

reduced these *a priori* uncertainties by a factor of five, roughly, bringing down those values to the levels shown in the third column of Table 4. The estimated differences between the ground-based determination of Ida and where we now believe Ida was actually located at the time of the encounter are tabulated in the fourth column of Table 4 [7]. The final determination of the radial component of Ida was in error by nearly the full extent of the radial error bar. This caused a larger than anticipated time-of-flight error. Fig. 14 also illustrates these uncertainties.

TABLE 4: *Ida Ephemeris Error (67% certainty)*

	A Priori	Pre-encounter	Post-encounter Change from Pre-encounter
R (km)	±243	±66	56 ± 40
T (km)	±660	±180	-75 ± 64
N (km)	±475	±121	14 ± 116
Encounter time (s)	±20	±5	4 ± 2

NOTE: fig. 14. Ida Ephemeris Error (67% certainty) **IN BACK OF DOCUMENT**

The path to Ida is shown in fig. 15. Four maneuvers were planned for the Earth to Ida leg. The determination of the orbit and the execution of maneuvers were sufficiently accurate during this time that two maneuvers, the first and last of this set, were cancelled. The two remaining maneuvers, TCM19 and TCM20, are shown in fig. 15. The Ida minus 15 day solution upon which the design of TCM20 was based included one single-frame mosaic image.

NOTE: fig. 15. Ida Encounter Dispersions (67% certainty) Ida-centered Earth Mean Ecliptic (1950) **IN BACK OF DOCUMENT**

At 16:52:04 UTC on August 28, 1993, with an uncertainty of 2.4 seconds, Galileo reached the point of closest approach to Ida. The spacecraft passed Ida 2 ± 19 km below the target altitude of 2400 km, but was 5 seconds later than the expected encounter time of 16:51:59 ± 4 seconds (estimated one week before the encounter). The unexpectedly large correction in the radial component of Ida's ephemeris was the source of this timing error.

Ida, and a companion satellite Dactyl, are shown in fig. 16. Dactyl, discovered during this encounter, is the first known natural satellite of an asteroid. Dactyl is about 1 km in diameter, while Ida has dimensions of 53x23x18 km, with a rotation period of 4.6 hours. Spectral observations indicate that Dactyl is a stony type asteroid like its primary. This photograph was shuttered at a range of 12,000 km.

NOTE: fig. 16. Ida and Dactyl **IN BACK OF DOCUMENT**

The significance of Dactyl's discovery lay in the clues suggested about Ida's composition. In principle, when one body orbits another, applying Kepler's Third Law of motion will yield the mass of the primary. Thus Dactyl should provide the mass of Ida and in turn yield an estimate for its bulk density.

Camera data returned from the encounter contained 47 images of Dactyl, although not all the images were suitable for orbit determination. Combining the satisfactory Dactyl images along with an estimate of Ida's volume deduced from Ida images, produced a preliminary estimate of Dactyl's orbit. The perspective was poor, however, since both the spacecraft and Dactyl lay very nearly in Ida's equatorial plane, and the solutions were indeterminate. Therefore to bound the possible orbits, Dactyl's orbit was parameterized over a range of likely Ida densities -- from 1.5 to 4.0 grams per cubic centimeter [8]. Thus for each density there existed a unique orbit, although over this range of densities the respective orbits differed significantly. Fig. 17 illustrates several of these orbit solutions [8]. The available observations (marked with an 'x') fit each of the hypothesized orbits equally well. But without more observations all orbits are equally valid.

NOTE: fig. 17. Possible Dactyl Orbits **IN BACK OF DOCUMENT**

A subset of possible orbits were selected by applying extant dynamical and observational constraints [9]. Those solutions yielded a best estimate for Ida's density ρ, of approximately $2 \leq \rho \leq 3$ grams per cubic centimeter [8]. These bounds are the first-ever quantitative estimate of a stony asteroid's density. Taking a specific density of 2.8 g cc^{-1}, Dactyl's orbit with respect to Ida displays the following characteristics. The orbit is nearly circular (about 82x98 km), with a period of 27 hours and an inclination of 8.5° to the Ida equator.

4.6 PROBE JUPITER ENCOUNTER

Jupiter, the ultimate destination, loomed beyond Ida. Almost two years would pass before the next major set of events -- the final targetting of the probe and its subsequent separation from the orbiter. That final targetting maneuver in April 1995, the twenty-third scheduled trajectory correction maneuver for Galileo, equalled 8 cm s^{-1} and targetted the probe sufficiently close to the required entry corridor that a subsequent maneuver scheduled two months later was determined to be unnecessary and was cancelled.

The Jupiter Bplane for the Galileo spacecraft pair around the time of probe release is shown in fig. 18. The trajectory followed by the pair shortly before separation (at the time of TCM23) is indicated in the figure. After release, the probe was predicted to fall within 100 km of the nominal target.

The target was defined in terms of six Jupiter-relative entry parameters. These parameters were latitude, longitude, speed, azimuth, time of entry, and the entry flight path angle at a reference altitude of 450 km. This latter parameter, defined as the angle between the relative velocity vector and the local horizontal, was critical and depended strongly on the impact parameter **B**. The relationship between the magnitude of **B** and the entry flight path angle γ is shown below [10].

$$\tan \gamma \approx \sin\tau \, [\cos\tau - (\omega h/v)]^{-1} \qquad (5)$$

where $$\tau = \arccos \{B \sqrt{[h(2\mu v_\infty^2 + h)]^{-1}}\}$$

and v_∞ = hyperbolic excess velocity, μ = gravitational constant of Jupiter, ω = rotation rate of Jupiter, v = inertial probe entry velocity, h = reference entry altitude. The requirements levied on probe entry limited the probe entry angle to a corridor between -7.2° and -10.0° (with a certainty of 99%).

The probe followed a ballistic trajectory to Jupiter (almost -- solar radiation forces acting on the probe were insignificant). The orbiter, in contrast, was subject to numerous predictable maintenance activities (including some small thrusting events) which significantly altered the ballistic trajectory the orbiter might otherwise have followed. The 'post-separation' trajectory of the orbiter in fig. 18 is the path the orbiter would follow to Jupiter in the absence of all future trajectory correction maneuvers (but inclusive of the "maintenance" activities). The 'spacecraft pair (no separation)' designation in fig. 18 is the hypothetical path the spacecraft would follow subject to the same conditions, if the probe failed to separate from the orbiter. Thus the difference between these latter two trajectories represents the net velocity change imparted to the orbiter by the release of the probe (estimated to equal 43.7 ± 0.4 mm s^{-1} (axially), about 2.5% lower than expected.)

NOTE: fig. 18. Probe Jupiter Encounter Dispersions (67% certainty) **IN BACK OF DOCUMENT**
December 5, 1995 22:00 UTC Jupiter-centered Earth Mean Ecliptic (1950)

Gravity focussing occurs when a large body is approached and the downtrack error in the trajectory is observed to increase (defocus), while the crosstrack error decreases (focuses) [described in an orthogonal rotating frame with the x axis parallel to the velocity vector (downtrack), the z axis normal to the plane-of-motion (out-of-plane), and the y axis normal to x and z (crosstrack)]. Gravity focussing is especially evident in fig. 18, where the reconstruction dispersion is compressed into a narrow, extended ellipse. The relationships describing focussing of the entry probe state (x,y,z) with respect to its initial state at minus infinity (x_∞, y_∞, z_∞) are as follows [11]:

$$\partial x/\partial x_\infty = \{1 - 2/[e\ \cosh(F) - 1]\}^{1/2} \quad (6)$$

$$\partial x/\partial y_\infty = -2e^{-1}(e^2 - 1)^{1/2}\ \exp(F)[e^2\ \cosh^2(F) - 1]^{1/2} \quad (7)$$

$$\partial y/\partial y_\infty = [e\ \cosh(F) - 1]^{1/2}\ [e\ \cosh(F) + 1]^{-1/2}\ [1 + e^{-1}\ \exp(F)] \quad (8)$$

$$\partial z/\partial z_\infty = |1 - e^{-1}\ \exp(F)| \quad (9)$$

where $$e\ \sinh(F) - F = (V_\infty^3/\mu)(t - t_{CA}) \quad (10)$$

and V_∞ = the hyperbolic excess velocity, e = the orbit eccentricity, t_{CA} = the time of closest approach, μ = Jupiter's gravity. (Note that equation (1) is a limiting result of (6) - (10).) From equations (6) - (10), the crosstrack focussing at closest approach was 0.25, the out-of-plane focussing was 0.0011, the downtrack defocussing was 8.0, and the coupling of crosstrack into downtrack was 2.0. Fig. 18, however, is a Bplane on December 5 -- two days before probe entry. (Since the probe plummets into Jupiter's atmosphere, configuring a Bplane at the time of closest approach is impractical.) Thus the full consequences of gravity focussing are not obvious in fig. 18.

The probe satisfied all targetting requirements, although it fell slightly beyond the dispersion region predicted just after separation. This marginal inconsistency is not fully understood, but mismodelling of the dynamics of probe-release is conjectured. Probe targetting history is summarized in Table 5 [12].

TABLE 5: *Probe Targeting History (67% Certainty)*

Delivery	Entry Time 12/7/95 UTC	Relative Flight-Path Angle (°)	Latitude (°)	Longitude (°)
Target	22:04:26.0 ± 188 s	–8.60 ± 0.55	6.57 ± 0.20	none
Pre-separation (TCM 23)	22:04:29.0 ± 37 s	–8.59 ± 0.15	6.57 ± 0.02	354.60 ± 0.46
Reconstruction	22:04:43.9 ± 3.1 s	–8.41 ± 0.04	6.54 ± 0.01	354.79 ± 0.09

A heliocentric view of the probe (and orbiter) trajectories at the time of arrival at Jupiter is shown in fig. 19.

NOTE: fig. 19. Probe Trajectory Approaching Jupiter (Heliocentric View) **IN BACK OF DOCUMENT**

4.7 ORBITER IO ENCOUNTER

Subsequent to probe-release the orbiter performed a large (61 m s^{-1}) orbit deflection maneuver (TCM25) to adjust the path of the orbiter toward an Io-centered target. One month later, a smaller (1 m s^{-1}) maneuver (TCM 26) was performed to refine the targetting. The Bplane intercept of this trajectory remained stable for three months. Not until two weeks before the encounter, when the signal tracking Galileo began to show significant increases in information content (a manifestation of Jupiter's gravity) did the solution demonstrate any meaningful movement.

Subsequent results remained stable for the remainder of the approach and were consistent with post-encounter reconstructions. The Io approach is shown in fig. 20.

NOTE: fig. 20. Orbiter Io Encounter Dispersions (67% certainty) Io-centered Earth Mean Ecliptic (1950) **IN BACK OF DOCUMENT**

Prior to the encounter in October a malfunctioning data recording system on the spacecraft prompted the project team to cancel plans for imaging at the Io encounter (science and navigation pictures). It followed that without the need to frame scenes, camera pointing accuracy was irrelevent. This led to *ad hoc* relaxed targetting requirements. Spacecraft energy change for orbit insertion became the sole driver of the encounter. The encounter was designed to occur at equatorial latitudes, so energy change was strongly correlated with altitude. B•T, proportional to altitude, also correlated with energy. The B•R component was less important due to focussing effects, and therefore latitude errors were not significant for an orbit energy change (to first order).[‡]

During the month preceding the Io encounter, estimates of the spacecraft orbit consistently placed it within ±150 km of the target altitude. The dearth of optical data meant the B•R uncertainty remained larger than originally forecast, but this was in a direction that was relatively unimportant now. (In general, while B•R knowledge improves slowly with additional doppler, the improvement is substantial with optical data.) On December 7, Io closest approach occurred at an altitude of 897.3 km ± 0.2, at a time of 17:45:58.4 UTC ± 0.01 s, 14 seconds after the target time.

The orbiter's blind (but not deaf) encounter with Io nevertheless provided an unprecedented opportunity to directly measure the location of Io relative to Earth. (The Io–spacecraft measurement was 540 times more sensitive than the one provided by Voyager.) This measurement was obtained by radiometric means during the flyby and indicated an error in Io's Jovicentric state at the time of the flyby of 9 km and 2 m s^{-1} (root-sum-square), with respect to the extant *a priori* Jet Propulsion Laboratory Jupiter satellite ephemeris, JUP076.

This flyby was also the first-ever sampling of Io's gravity field. The gravity signature of Io acquired during the encounter with respect to the *a priori* nominal field is reproduced in fig. 21. From analysis of the data, the following parameters for Io were estimated: mass (GM_{Io}), and the low order spherical harmonic terms J_2, C_{22}, and S_{22}. The results of this gravity field determination are outlined in Table 6 [12].

[‡] Without Io imaging, acceptable limits on altitude were ±≈100 km with no bounds on encounter time (to first order).

NOTE: Fig. 21. Gravity Signal at Io Closest Approach **IN BACK OF DOCUMENT**

TABLE 6: *Io Gravity Results (67% certainty)*

Flyby Altitude (km)	J_2 $\times 10^{-6}$	C_{22} $\times 10^{-6}$	S_{22} $\times 10^{-6}$	GM_{Io} ($km^3\ s^{-2}$)	Io Adjustment (km)
897.3 ± 0.2	1863 ± 423	547 ± 14	19 ± 12	5960.3 ± 0.5	9 ± 9

The observed value for C_{22} is related to the structure of Io by equating the difference in the equatorial moments of inertia with its rotation rate:

$$C_{22} = (B - A) / (4mr^2) \qquad C_{22} = (3/4)\alpha q \qquad (11)$$

where the satellite's principal moments of inertia are A, B (and C -- not shown), m equals the satellite's mass, r is its mean radius, $q = a_c / g_{Io}$, the ratio of centrepital acceleration to gravitational acceleration at the equator, and α (a dependent variable) a dimensionless coefficient ($\alpha = 0.5$ for constant density).

While these results are still preliminary, the solution to (11) suggests a differentiated structure for Io. That is, the evidence indicates that Io contains an iron or iron-sulphide core with a radius of approximately 50% the satellite radius [13]. Corroborating information was supplied by the Galileo magnetometer. A magnetic signature above Io was observed that was interpreted as an intrinsic magnetic field anti-aligned with Jupiter's magnetic dipole [14]. This result is consistent for a body with a differentiated core.

Jupiter's ephemeris shifted significantly in position from the latest pre-Galileo Jet Propulsion Laboratory planetary ephemeris, DE-143. These corrections are listed in Table 7 [12]. (The explanation for this unexpectedly large adjustment will be the subject of a forthcoming paper.) The precision of this measurement has improved significantly from previous determinations by the Pioneer, Voyager, and Ulysses spacecraft. Radial uncertainty decreased by a factor of five and downtrack uncertainty improved seven-fold, with respect to DE-143. Jupiter's out-of-plane (normal) error improved by a factor of four.

TABLE 7: *Jupiter Ephemeris Error (67% Certainty)*
Sun-centered, Earth Mean Ecliptic (1950), Jupiter-orbit Fixed

	A Priori (DE143)	Post-encounter Change from *A Priori*
R (km)	±14.1	18.8 ± 3.0
T (km)	±51.4	–69.3 ± 7.4
N (km)	±344.0	549.4 ± 88.2

Revised estimates for a subset of Jupiter's gravity parameters, i.e., GM_{Jup}, J_2, J_4, are also listed here. Jupiter GM was estimated to equal 126,712,718 ± 85 km^3s^{-2}—a value within the uncertainty quoted by Campbell and Synnott [15]. The tabulated values of J_2 and J_4 do not differ from values in the literature, although the precision of the estimate has improved. The updated values and uncertainties are listed in Table 8 [12].

TABLE 8: *Jupiter Gravity (67% Certainty)*

GM_{Jup} (km^3s^{-2})	J_2 $\times 10^{-6}$	J_4 $\times 10^{-6}$
126,712,718 ± 85	14,736 ± 0.5	−587 ± 2.5

5. DISCUSSION

By and large, ephemeris uncertainty dominated navigation error at the target. *A priori* planetary uncertainties ranged from 2 km at Earth to 350 km at Jupiter, while the *a priori* Io orbit error with respect to Jupiter was 90 km. In general, ephemeris uncertainty correlates with proximity to Earth since, for similar numbers of observations, closer bodies have better determined ephemerides than more distant objects. This result is no surprise; however it ignores spaceraft-relative imaging. The failure of the high-gain antenna to deploy significantly restricted the number of navigation images shuttered by Galileo, leaving navigation mostly dependent upon the radio subsystem and *a priori* ephemerides. This was particularly true for the Io encounter. Large orbit uncertainties in turn corresponded roughly with increased trajectory error at the target, in agreement with the statistical expectation.

An exception was the Earth-1 encounter, which experienced a relatively large trajectory error. In comparison with the Earth-2 experience, the Earth-1 orbit errors were nearly a factor of three larger at the time of the final pre-encounter maneuver. Both deliveries contained equal numbers of ΔDOR observations over similar time spans (the time span of observations for the Earth-1 encounter was actually about 50% longer). The defining difference between the two encounters was the declination of the spacecraft on approach. For the first Earth encounter, the spacecraft's declination was about 14° on its approach asymptote. At the second encounter the spacecraft lay at approximately 20° during the analogous time span. The relatively poor delivery at Earth-1 can, at least in part, be attributed to the low declination of the spacecraft. This, combined with an insufficient number of ΔDOR observations over the pertinent period, contributed to the pre-Earth-1 trajectory mismodelling.

6. SUMMARY

The Galileo orbiter and probe successfully achieved their respective Jovian objectives in December 1995, after a voyage of six years. The performance of the navigation subsystem underscored the scale of this undertaking. While the system fell short of predicting statistically consistent results for all maneuvers, nevertheless it performed within expectations and delivered Galileo to Jupiter with sufficient propellant to continue the mission. (The spacecraft entered orbit with 291 kg of propellant versus an expected orbital propellant mass, at launch, of 303 kg -- in spite of expending an unanticipated 51 kg in efforts to free the stuck high gain antenna.) The probe performed nearly flawlessly, and the orbiter entered a near nominal orbit around Jupiter. Subsequently, the orbiter began preparations for a series of frequent encounters with the three remaining major Jovian satellites, to begin in June 1996.

6. AKNOWLEDGEMENT

The work described in this paper was performed at the Jet Propulsion Laboratory, California Institute of Technology, under a contract with the National Aeronautics and Space Administration. The authors of this paper represent only a subset of the Galileo Navigation Team. Navigation personnel at the time of the Io encounter (excluding the authors) were: W.E. Kirhofer (team leader), L.A. D'Amario, D.V. Byrnes, G.J. Garner, C.A. Halsell, J.R. Johannesen, R.A. Mase, J.M. Neff, J.L. Pojman, C.L. Potts, and M.G. Wilson. Many thanks to C.L. Potts for helping with the graphics and for supplying the mission propellant cost contour plots.

Donald Yeomans and Paul Chodas supplied the Gaspra and Ida ephemerides, and Robert Jacobson the Io ephemeris. The authors would also like to thank B.G. Williams for his helpful comments.

REFERENCES

1. In 1986, after the *Challenger* loss, NASA placed Galileo onto a less volatile and less powerful booster out of concern for the safety of the Shuttle crew.

2. Galileo observed the G, H, K, L, Q1 and W impacts between July 18 and July 22. Also see, A.P. Ingersoll and H. Kanamori, *Nature*, **374**, 706 (1995).

3. Galileo probe issue, *Science*, **272**, 837 (1996).

4. T.W. Hamilton and W.G. Melbourne, "Information Content of a Single Pass of Doppler Data from a Distant Spacecraft", in *The Deep Space Network Space Programs Summary 37-39*, Vol. III, pp. 18-23, Jet Propulsion Laboratory, Pasadena, California, May 31, 1966.

5. E.H. Maize, "Earth Flyby Delivery Strategies for the Galileo Mission", *Astrodynamics 1989: Proceedings of the AAS/AIAA Astrodynamics Specialist Conference*, Univelt, San Diego, California, 1990.

6. P.H. Kallemeyn, R.J. Haw, V.M. Pollmeier, F.T. Nicholson, "Galileo Orbit Determination for the Gaspra Asteroid Encounter", *Proceedings of the 1992 AIAA/AAS Astrodynamics Conference*, AIAA, New York, NY, 1992.

7. P.G. Antreasian, F.T. Nicholson, P.H. Kallemeyn, S. Bhaskaran, R.J Haw, P. Halamek, "Galileo Orbit Determination for the Ida Encounter", *Advances in the Astronautical Sciences 1994*, Vol. 87, Part 2, Univelt, San Diego, California, 1994, pp. 1027–1048.

8. D.V. Byrnes, L.A. D'Amario, "Dactyl Orbit Determination Analysis," *Astrodynamics 1995: Proceedings of the AAS/AIAA Astrodynamics Specialist Conference*, Univelt, San Diego, California, 1996.

9. M.J.S. Belton et al, "Bulk density at asteroid 243 Ida from the orbit of its satellite Dactyl", *Nature*, **374**, 1995.

10. L.J. Miller, J.K. Miller, W.E. Kirhofer, "Navigation of the Galileo Mission", presented at AIAA 21st Aerospace Sciences Meeting, Reno NV, January 10-13, 1983.

11. R.K. Russell, "Gravity Focusing of Hyperbolic Trajectories", Internal Office Technical Memorandum 391-424, Jet Propulsion Laboratory, Pasadena, California, March 30, 1973.

12. R.J. Haw, P.G. Antreasian, E.J. Graat,T.P. McElrath, F.T. Nicholson, "Navigating Galileo at Jupiter", submitted to *Journal of Spacecraft and Rockets*, AIAA, Reston, VA, 1996.

13. J.D. Anderson, W.L. Sjogren, G. Schubert, "Galileo Gravity Results and the Internal Structure of Io", *Science*, **272**, 709 (1996).

14. M.G. Kivelson et al, ""Io's Interaction with the Plasma Torus: Galileo Magnetometer Report", *Science*, **274**, 396 (1996).

15. J.K. Campbell, S.P. Synnott, "Gravity Field of the Jovian System from Pioneer and Voyager Tracking Data", *The Astronomical Journal*, Vol. 90, No. 2, February 1985, pp. 364–372.

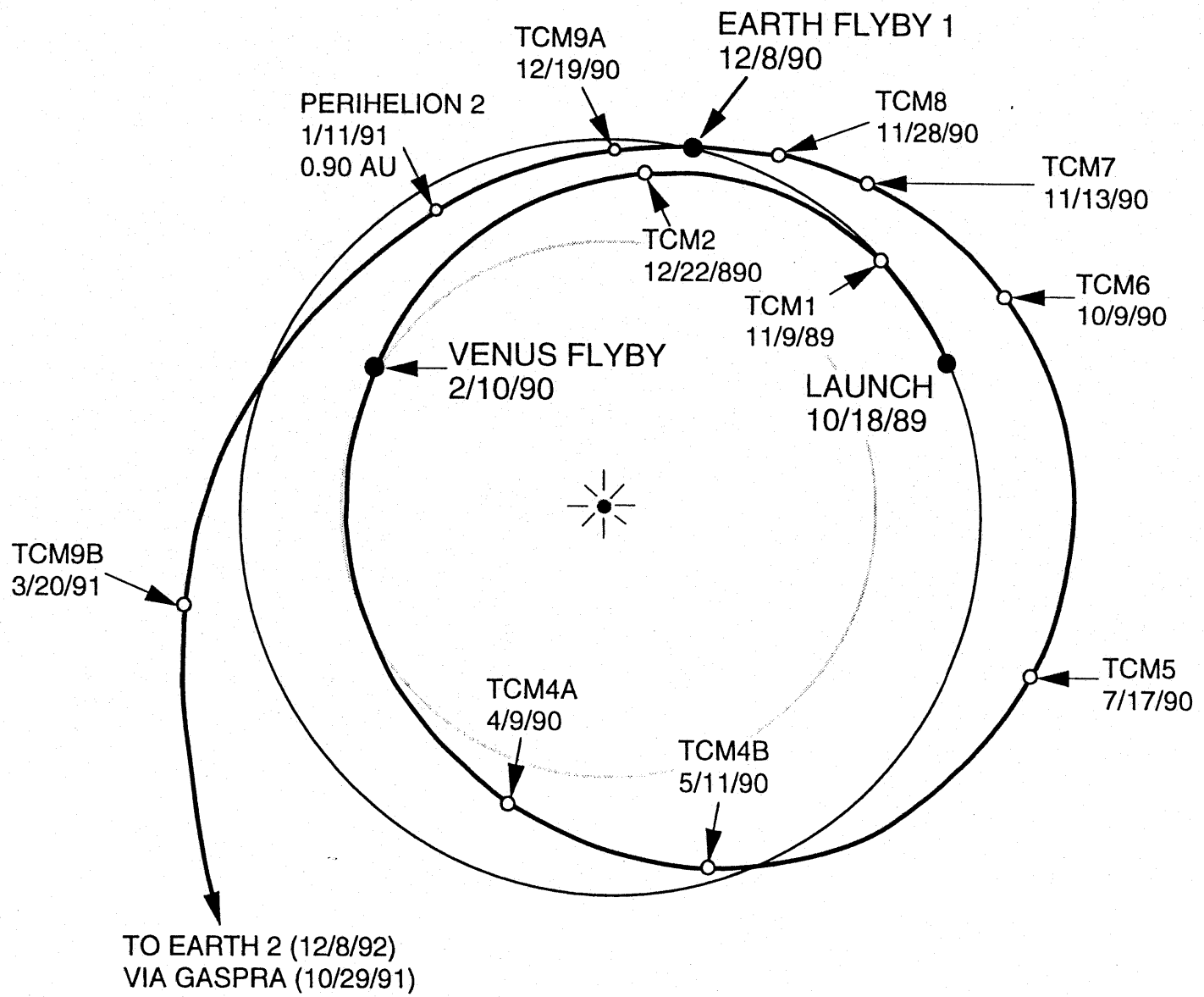
TCM9A
12/19/90
EARTH FLYBY 1
12/8/90
PERIHELION 2
1/11/91
0.90 AU
TCM8
11/28/90
TCM7
11/13/90
TCM2
12/22/890
TCM1
11/9/89
TCM6
10/9/90
VENUS FLYBY
2/10/90
LAUNCH
10/18/89
TCM9B
3/20/91
TCM5
7/17/90
TCM4A
4/9/90
TCM4B
5/11/90
TO EARTH 2 (12/8/92)
VIA GASPRA (10/29/91)

Fig 1

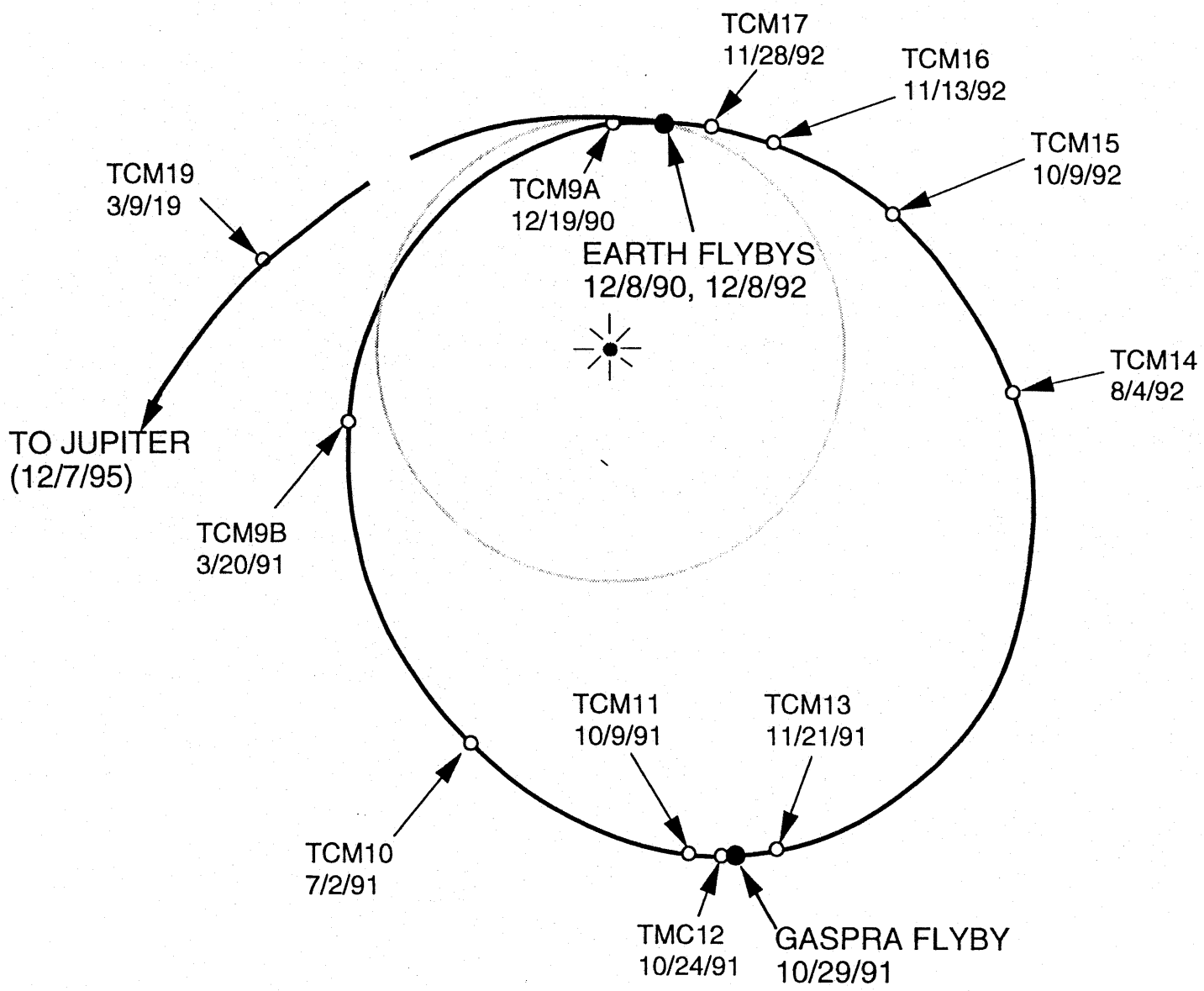
TCM17
11/28/92
TCM16
11/13/92
TCM15
10/9/92
TCM14
8/4/92
TCM13
11/21/91
TCM11
10/9/91
TCM10
7/2/91
TCM9B
3/20/91
TO JUPITER
(12/7/95)
TCM19
3/9/19
TCM9A
12/19/90
EARTH FLYBYS
12/8/90, 12/8/92
TMC12
10/24/91
GASPRA FLYBY
10/29/91

Fig 2

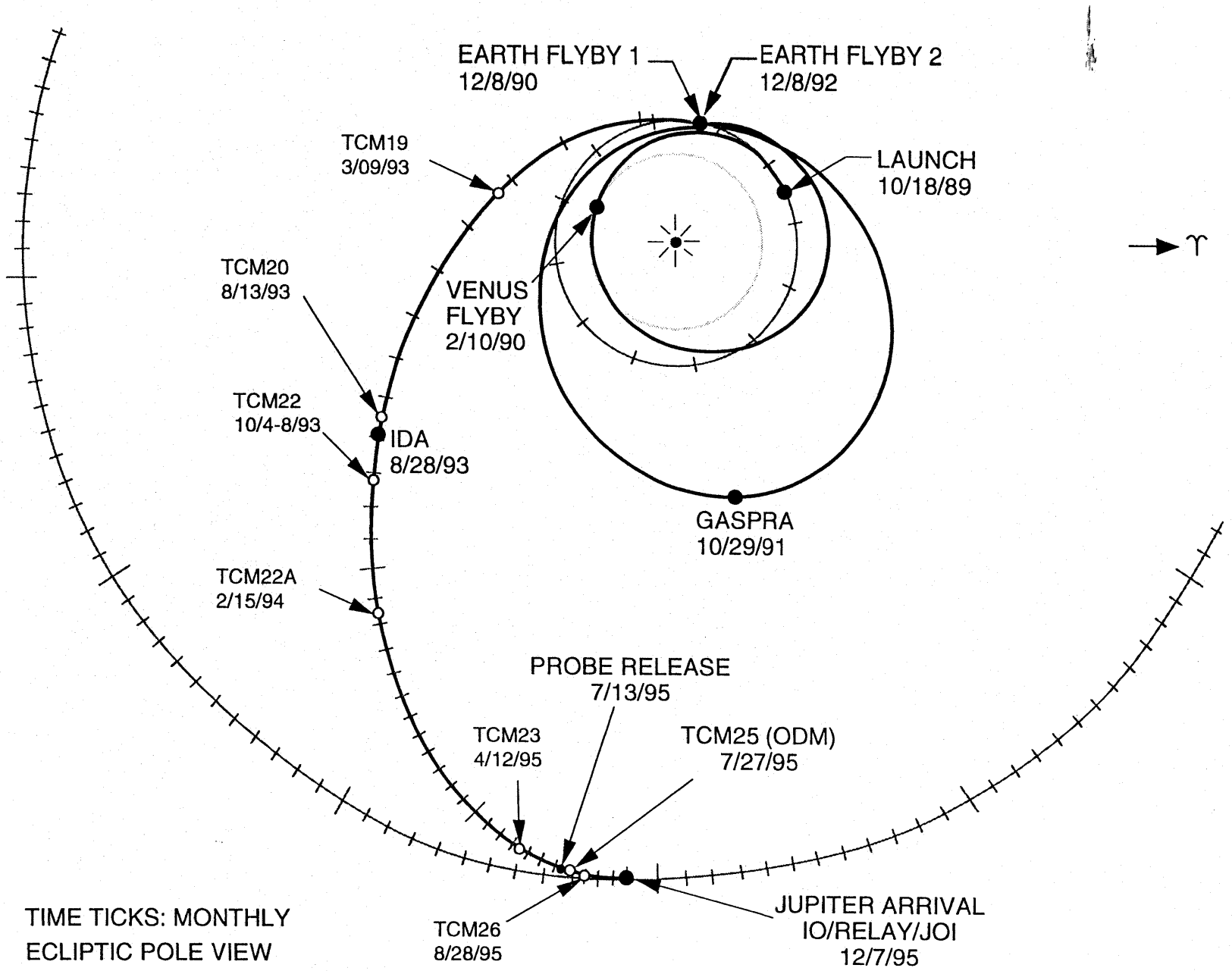
EARTH FLYBY 1
12/8/90
EARTH FLYBY 2
12/8/92
TCM19
3/09/93
LAUNCH
10/18/89
TCM20
8/13/93
VENUS
FLYBY
2/10/90
TCM22
10/4-8/93
IDA
8/28/93
GASPRA
10/29/91
TCM22A
2/15/94
PROBE RELEASE
7/13/95
TCM23
4/12/95
TCM25 (ODM)
7/27/95
TCM26
8/28/95
JUPITER ARRIVAL
IO/RELAY/JOI
12/7/95
TIME TICKS: MONTHLY
ECLIPTIC POLE VIEW

Fig 3

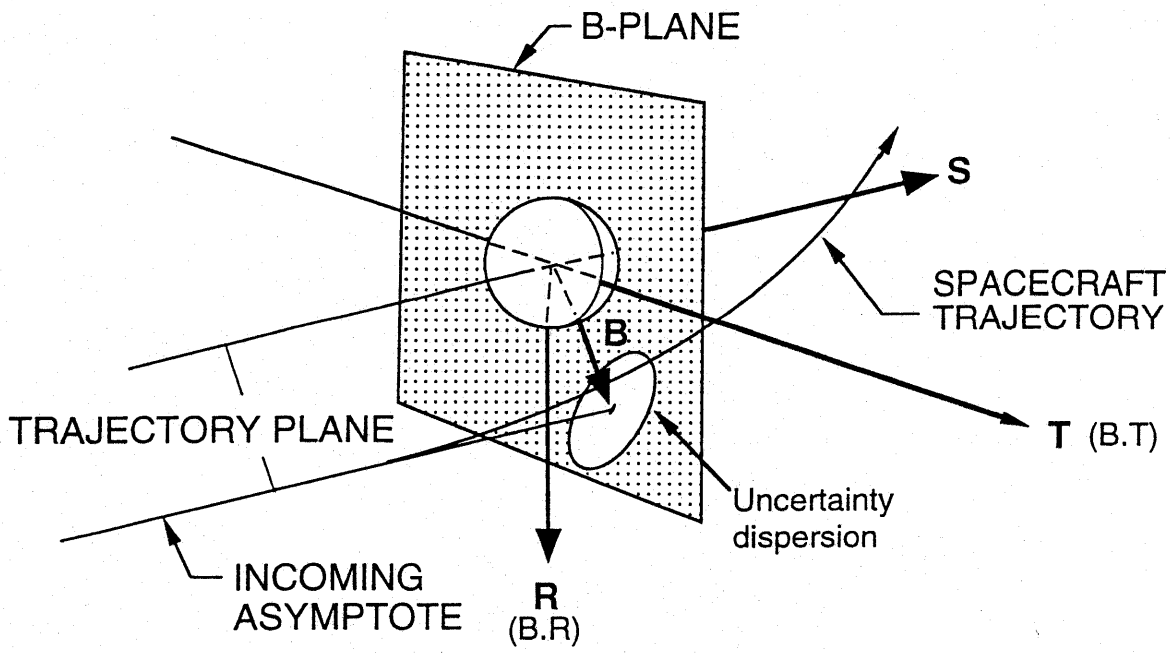

Figure 4; Geometry of the B-plane

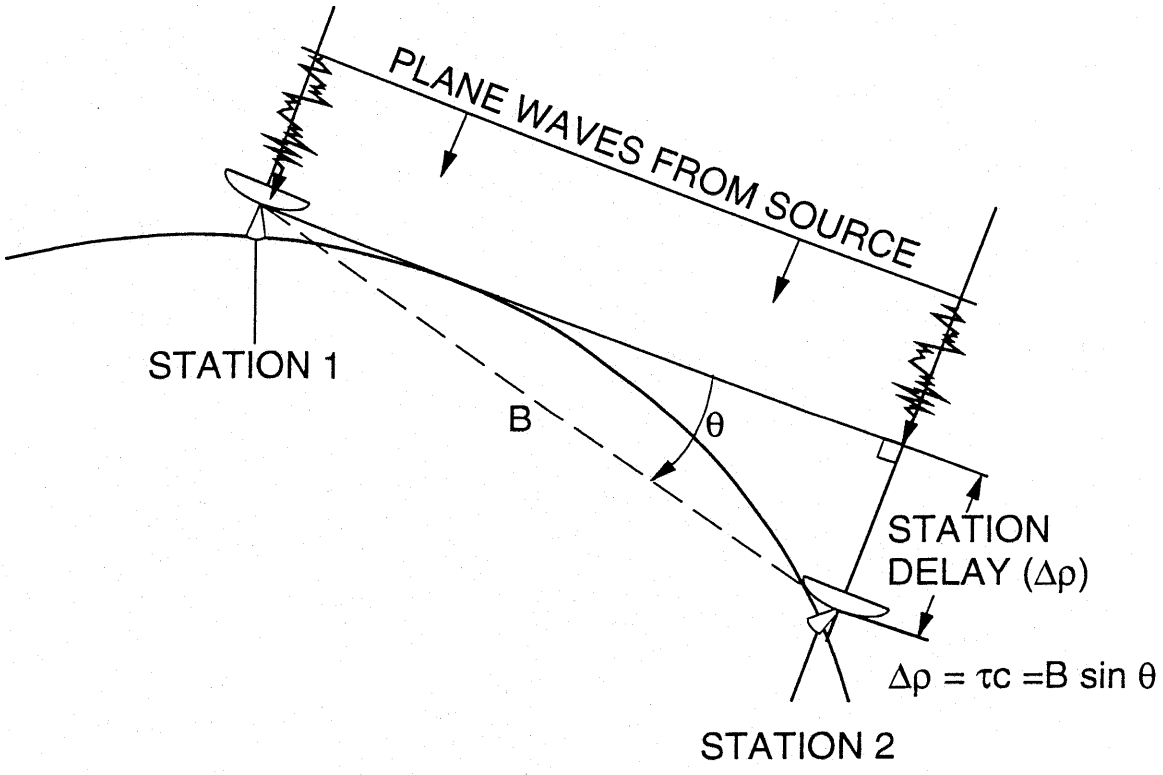

Figure 5. Observing geometry for VLBI data

Figure 4. IUS Injection Dispersions, 1.5σ, 67%

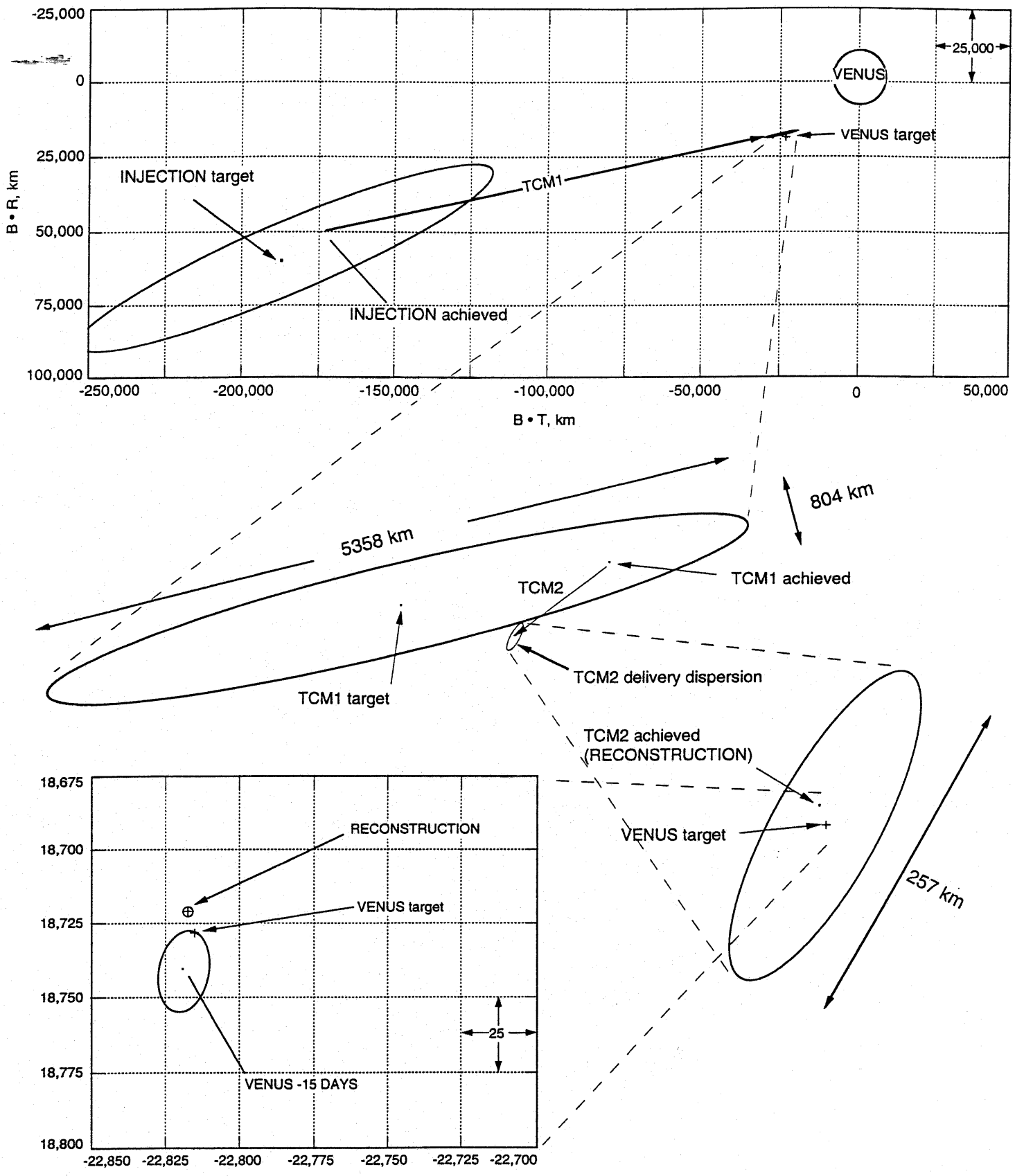

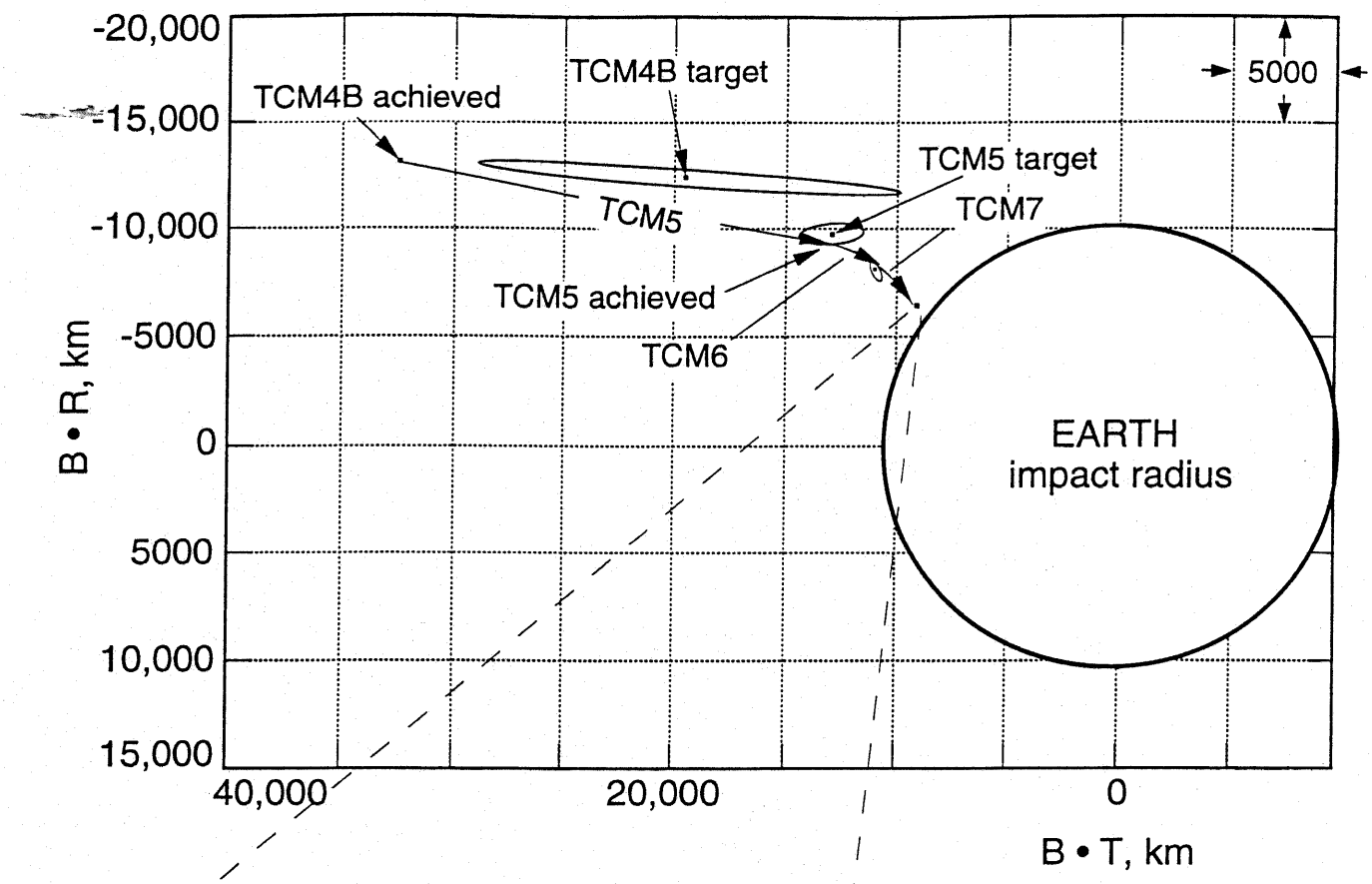
-20,000
-15,000
-10,000
-5000
0
5000
10,000
15,000
40,000
20,000
0
B • R, km
B • T, km
5000
TCM4B achieved
TCM4B target
TCM5
TCM5 target
TCM7
TCM5 achieved
TCM6
EARTH
impact radius

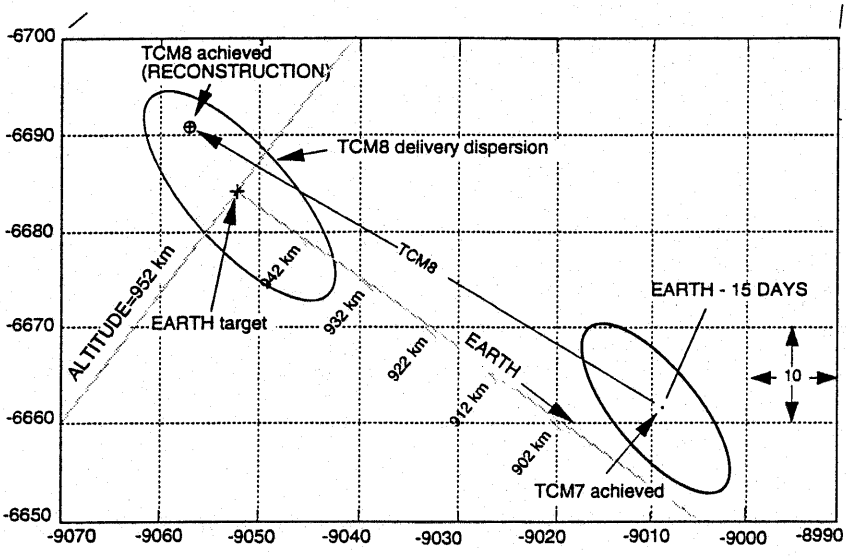
-6700
-6690
-6680
-6670
-6660
-6650
-9070
-9060
-9050
-9040
-9030
-9020
-9010
-9000
-8990
TCM8 achieved
(RECONSTRUCTION)
TCM8 delivery dispersion
ALTITUDE=952 km
942 km
EARTH target
932 km
TCM8
922 km
EARTH
912 km
902 km
EARTH - 15 DAYS
10
TCM7 achieved

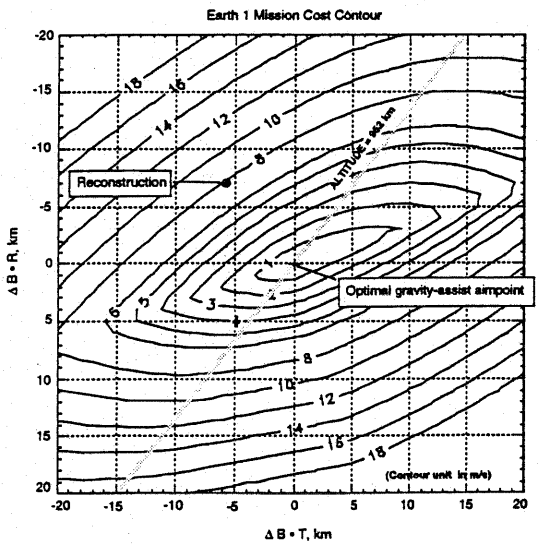
Earth 1 Mission Cost Contour
Reconstruction
Optimal gravity-assist aimpoint
ΔB • R, km
ΔB • T, km

figure 7

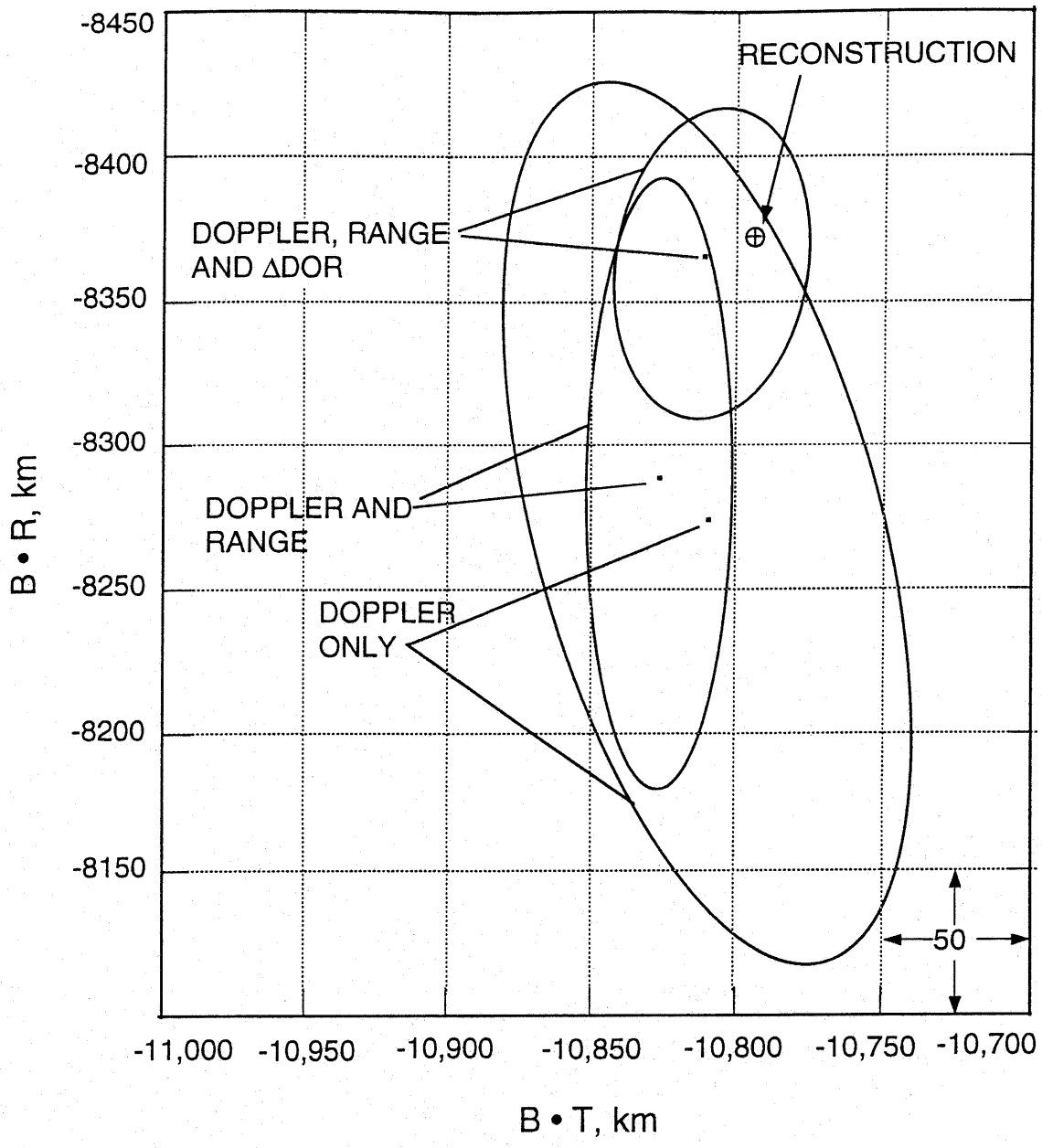

Figure 8 Earth1 - 40 Days EMO50

Fig 8

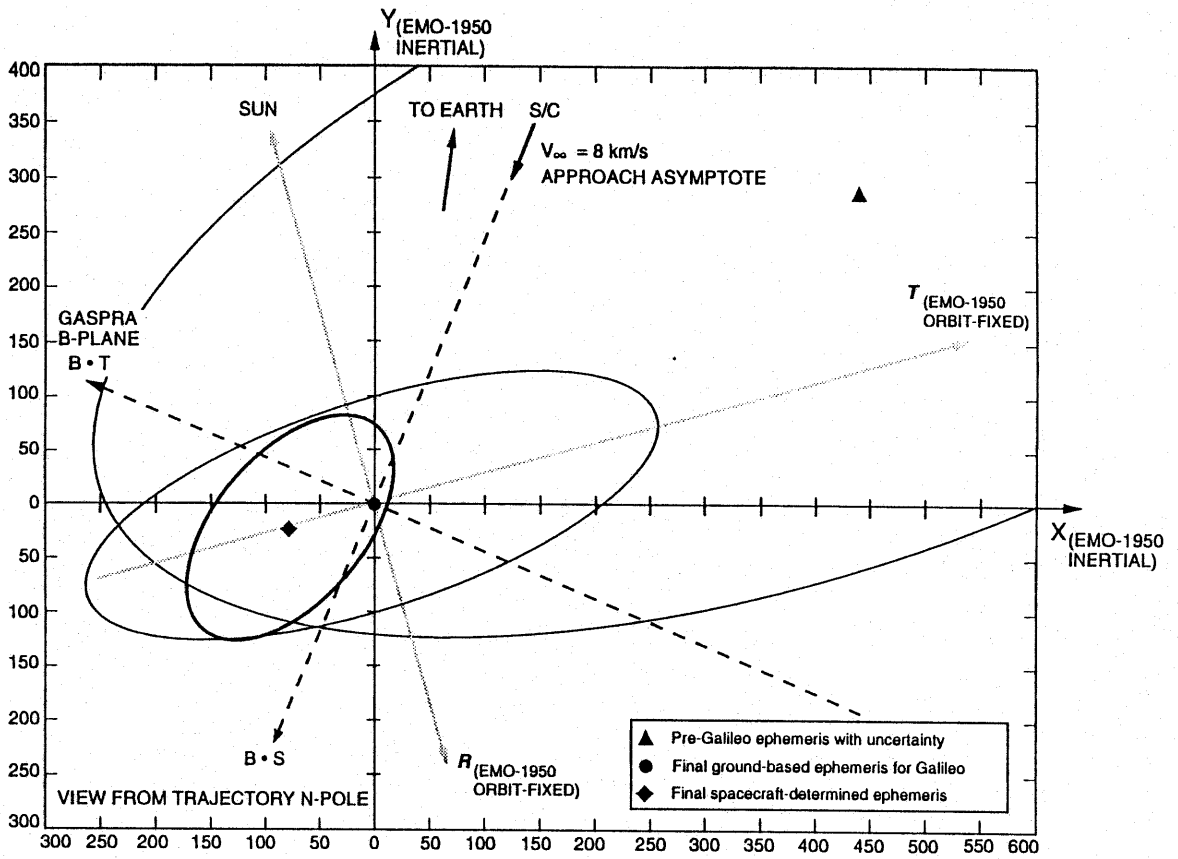
Y (EMO-1950 INERTIAL)
SUN
TO EARTH
S/C
V∞ = 8 km/s
APPROACH ASYMPTOTE
GASPRA
B-PLANE
B • T
T (EMO-1950 ORBIT-FIXED)
X (EMO-1950 INERTIAL)
B • S
R (EMO-1950 ORBIT-FIXED)
VIEW FROM TRAJECTORY N-POLE
Pre-Galileo ephemeris with uncertainty
Final ground-based ephemeris for Galileo
Final spacecraft-determined ephemeris
400
350
300
250
200
150
100
50
0
50
100
150
200
250
300
300 250 200 150 100 50 0 50 100 150 200 250 300 350 400 450 500 550 600

figure 9

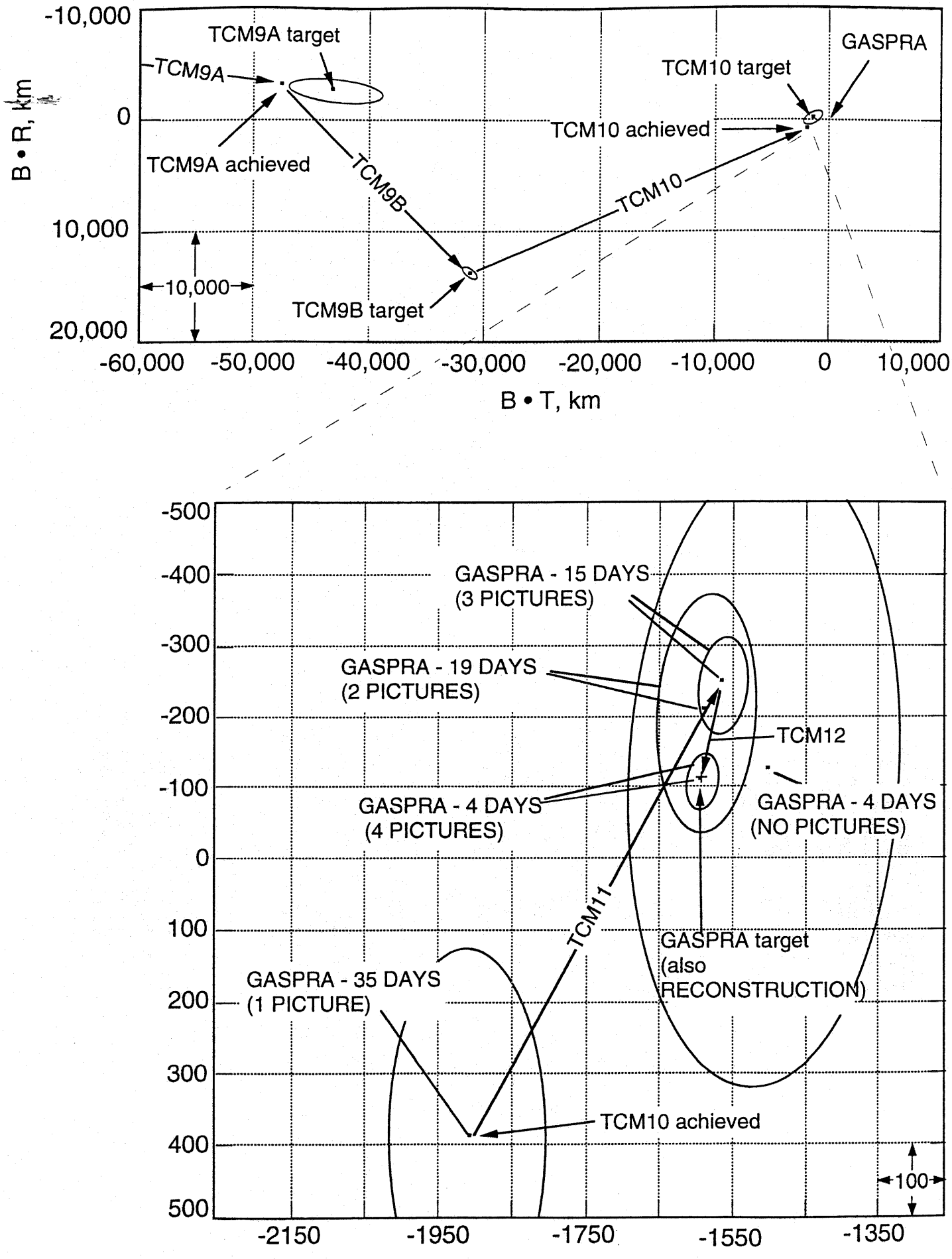
-10,000
0
10,000
20,000
B • R, km
TCM9A target
TCM9A
TCM9A achieved
TCM9B
TCM9B target
TCM10 target
GASPRA
TCM10 achieved
TCM10
10,000
-60,000
-50,000
-40,000
-30,000
-20,000
-10,000
0
10,000
B • T, km
-500
-400
-300
-200
-100
0
100
200
300
400
500
GASPRA - 15 DAYS
(3 PICTURES)
GASPRA - 19 DAYS
(2 PICTURES)
TCM12
GASPRA - 4 DAYS
(4 PICTURES)
GASPRA - 4 DAYS
(NO PICTURES)
TCM11
GASPRA target
(also
RECONSTRUCTION)
GASPRA - 35 DAYS
(1 PICTURE)
TCM10 achieved
100
-2150
-1950
-1750
-1550
-1350

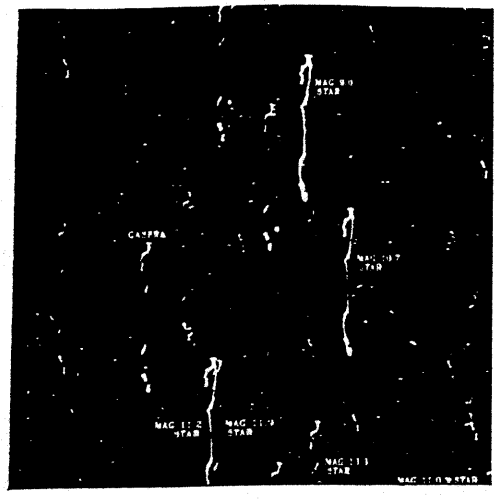

OPNAV 1

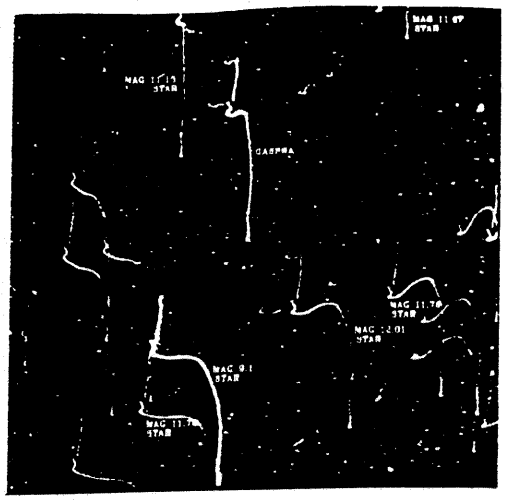

OPNAV 3

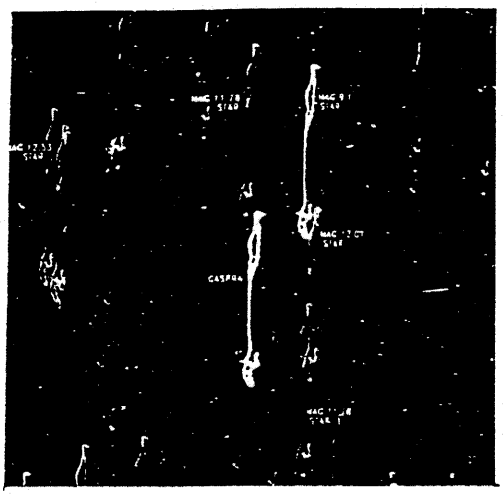

OPNAV 4

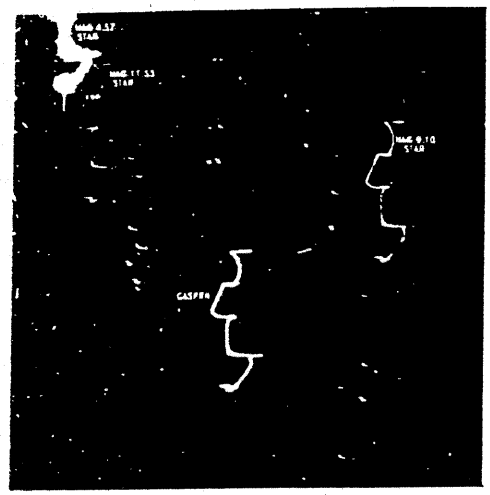

OPNAV 5

11
Figure : OPNAV Images

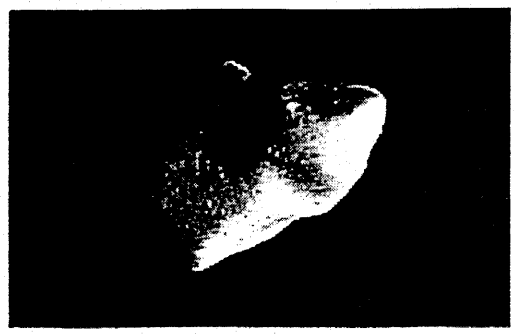

12
Figure First received science image of Gaspra,
one of four images comprising the four-color mosaic

Figure 13. Effect of the TCMs on the trajectory in the Earth2 B-plane

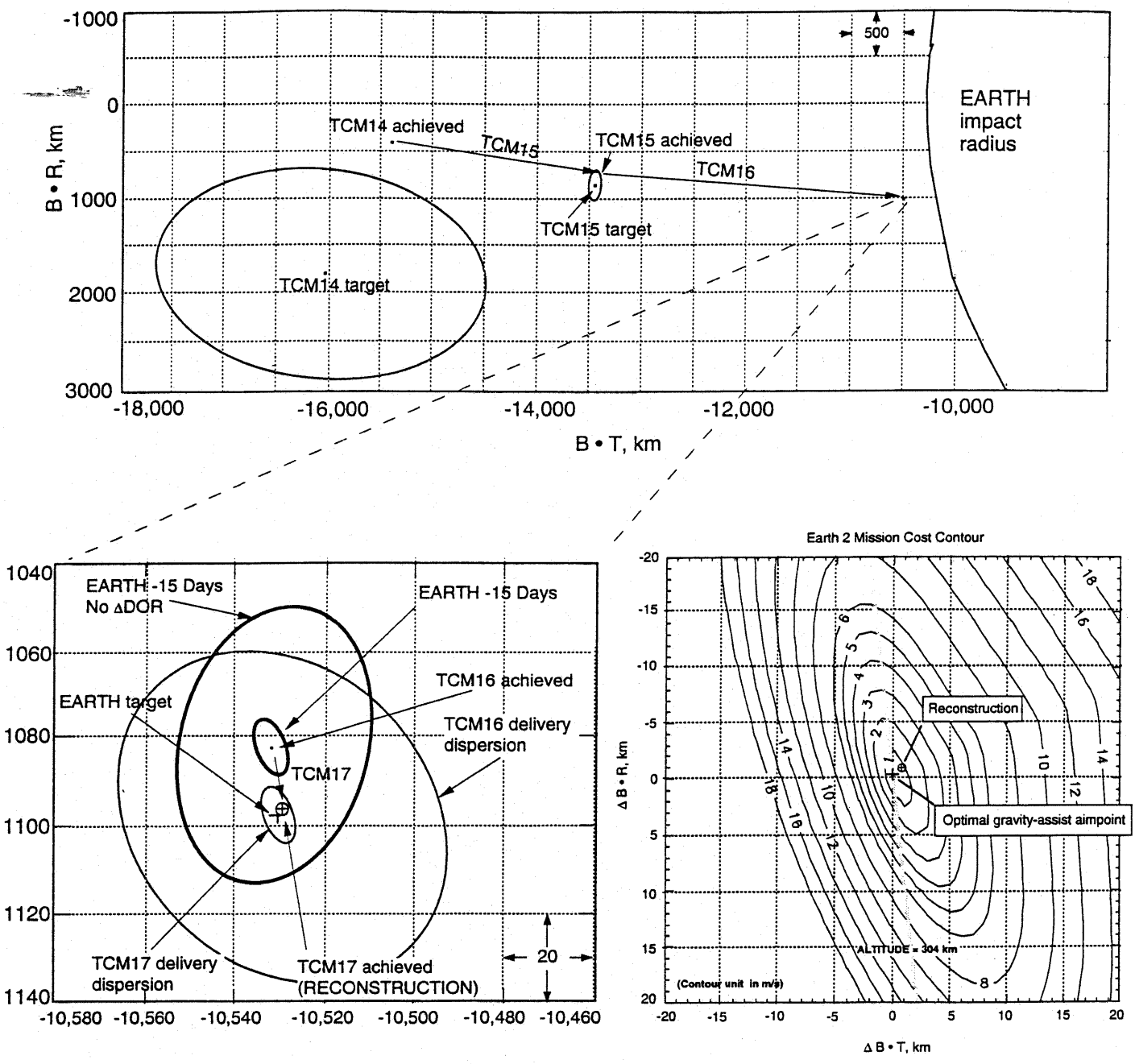

Fig 13

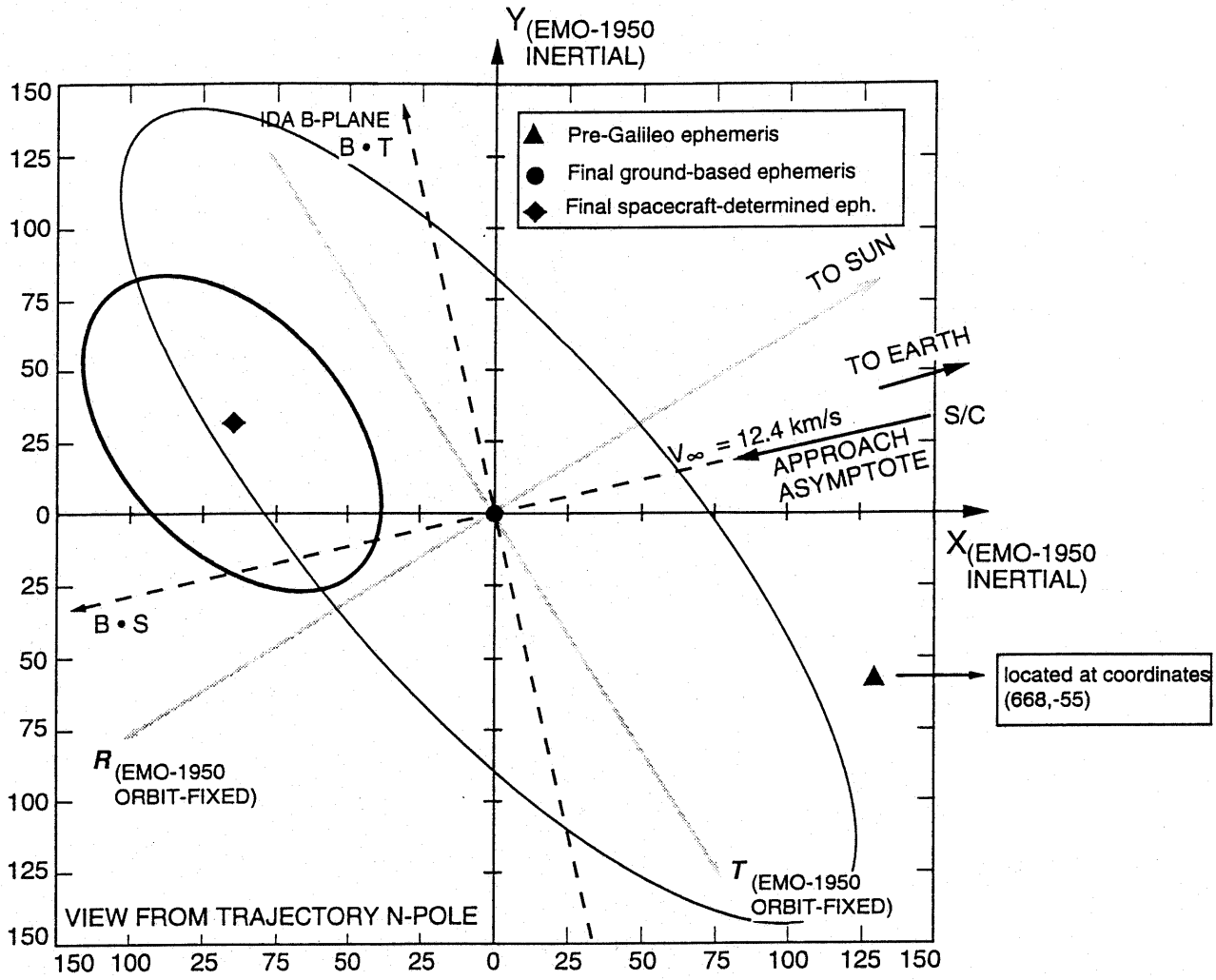
Y (EMO-1950 INERTIAL)
IDA B-PLANE
B • T
Pre-Galileo ephemeris
Final ground-based ephemeris
Final spacecraft-determined eph.
TO SUN
TO EARTH
S/C
V∞ = 12.4 km/s
APPROACH ASYMPTOTE
X (EMO-1950 INERTIAL)
B • S
located at coordinates (668,-55)
R (EMO-1950 ORBIT-FIXED)
T (EMO-1950 ORBIT-FIXED)
VIEW FROM TRAJECTORY N-POLE
150 100 25 75 50 25 0 25 50 75 100 125 150

figure 14

Figure 15. Ida-centered B-plane EME 1950

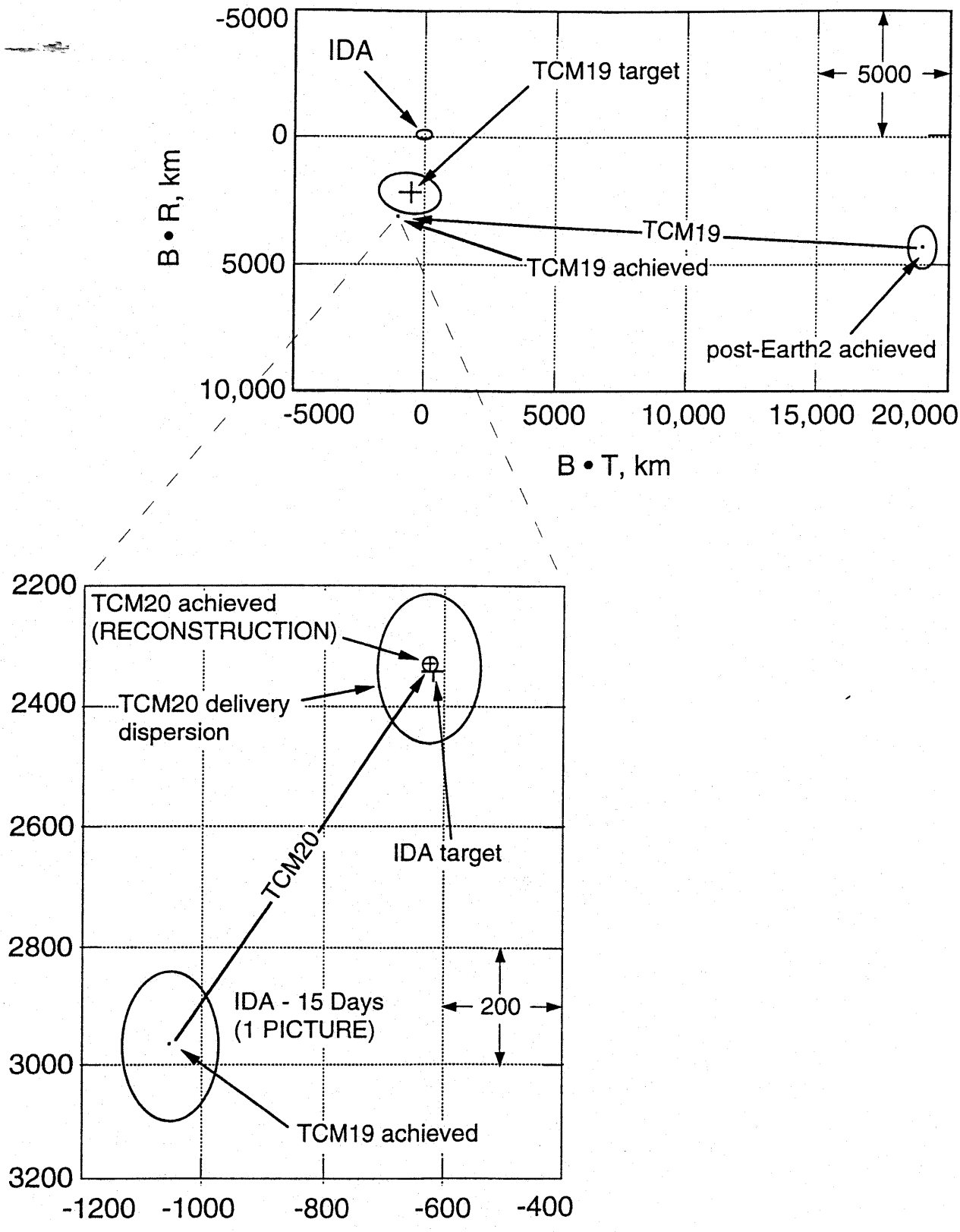

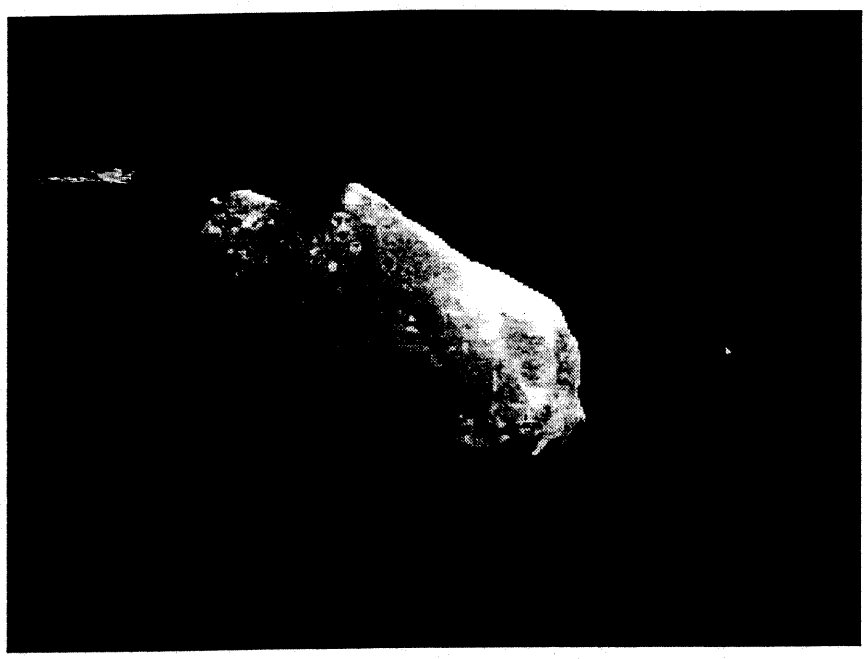

Fig 16

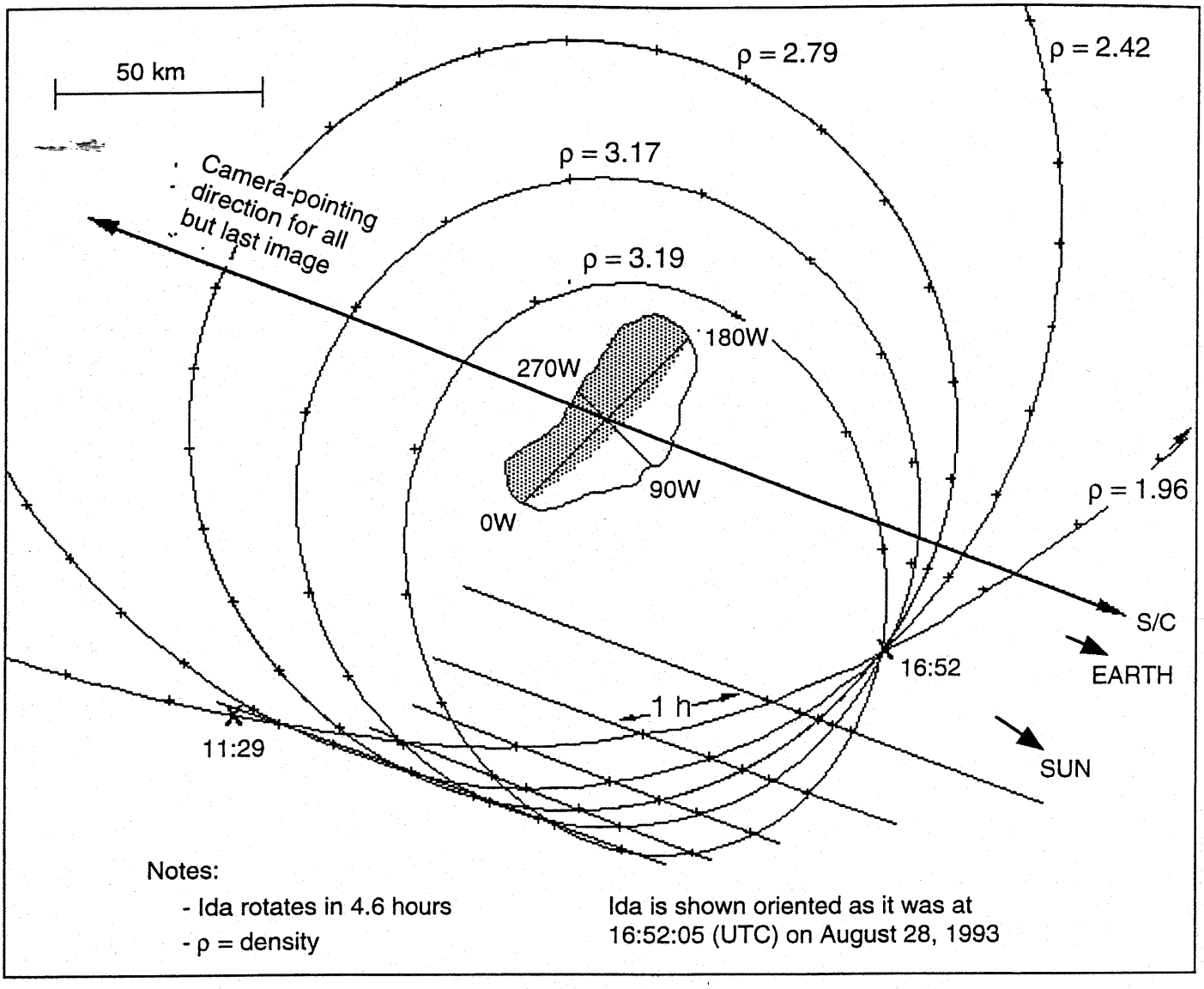
50 km
ρ = 2.79
ρ = 2.42
ρ = 3.17
Camera-pointing direction for all but last image
ρ = 3.19
180W
270W
90W
0W
ρ = 1.96
S/C
EARTH
16:52
1 h
11:29
SUN
Notes:
- Ida rotates in 4.6 hours
- ρ = density
Ida is shown oriented as it was at
16:52:05 (UTC) on August 28, 1993

Fig. 17

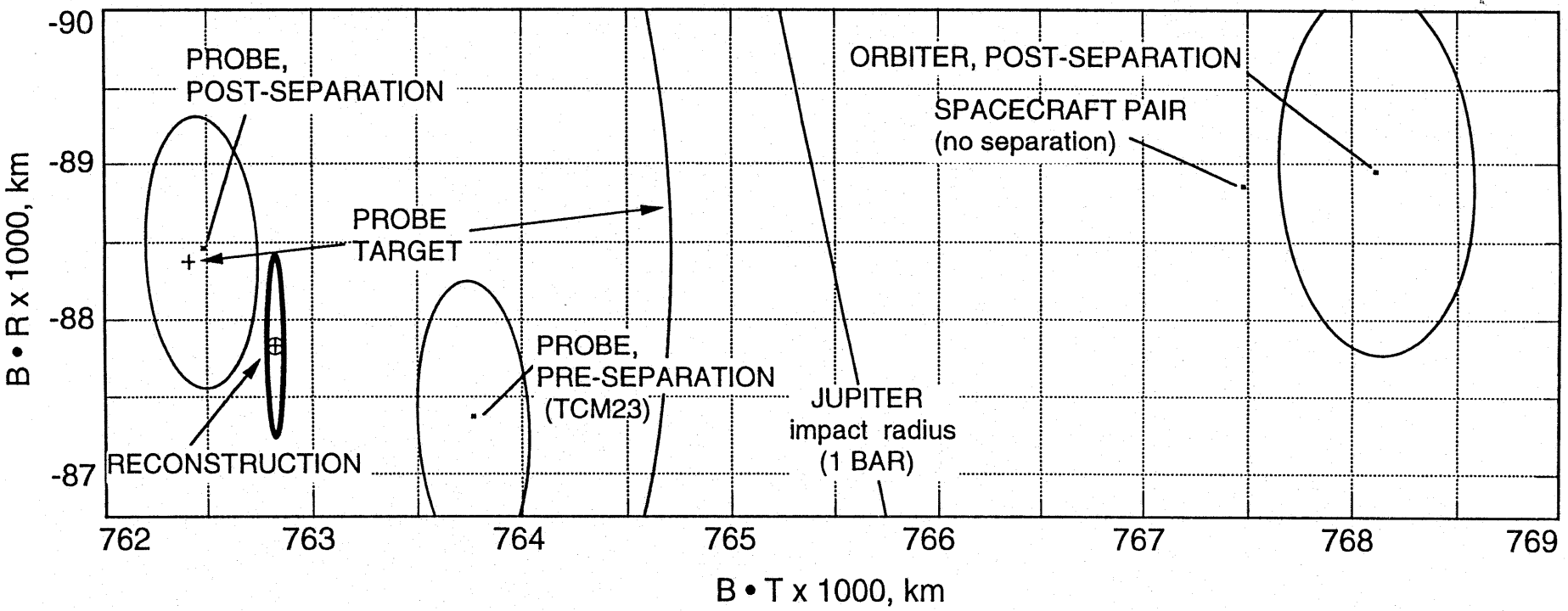

Figure 18
on Dec 5, 1995

Fig 18

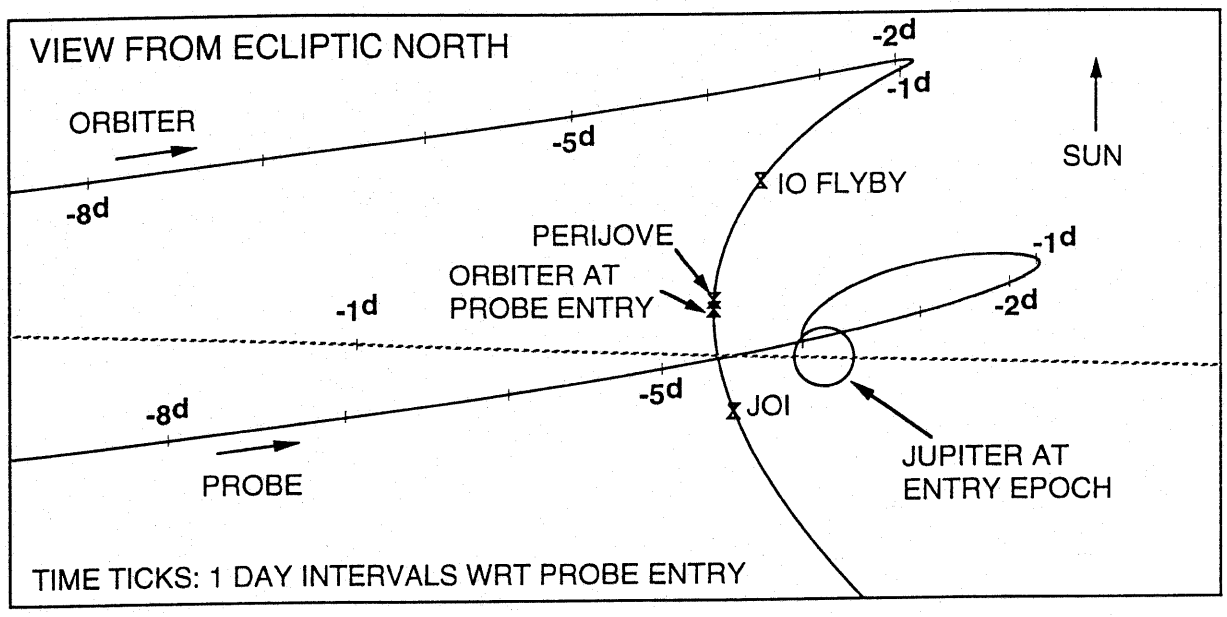
VIEW FROM ECLIPTIC NORTH
ORBITER
-8d
-5d
-2d
-1d
IO FLYBY
SUN
PERIJOVE
ORBITER AT
PROBE ENTRY
-1d
-1d
-2d
-8d
-5d
JOI
PROBE
JUPITER AT
ENTRY EPOCH
TIME TICKS: 1 DAY INTERVALS WRT PROBE ENTRY

Fig 19

~~Figure 21~~. Io-centered EMO50 B-plane

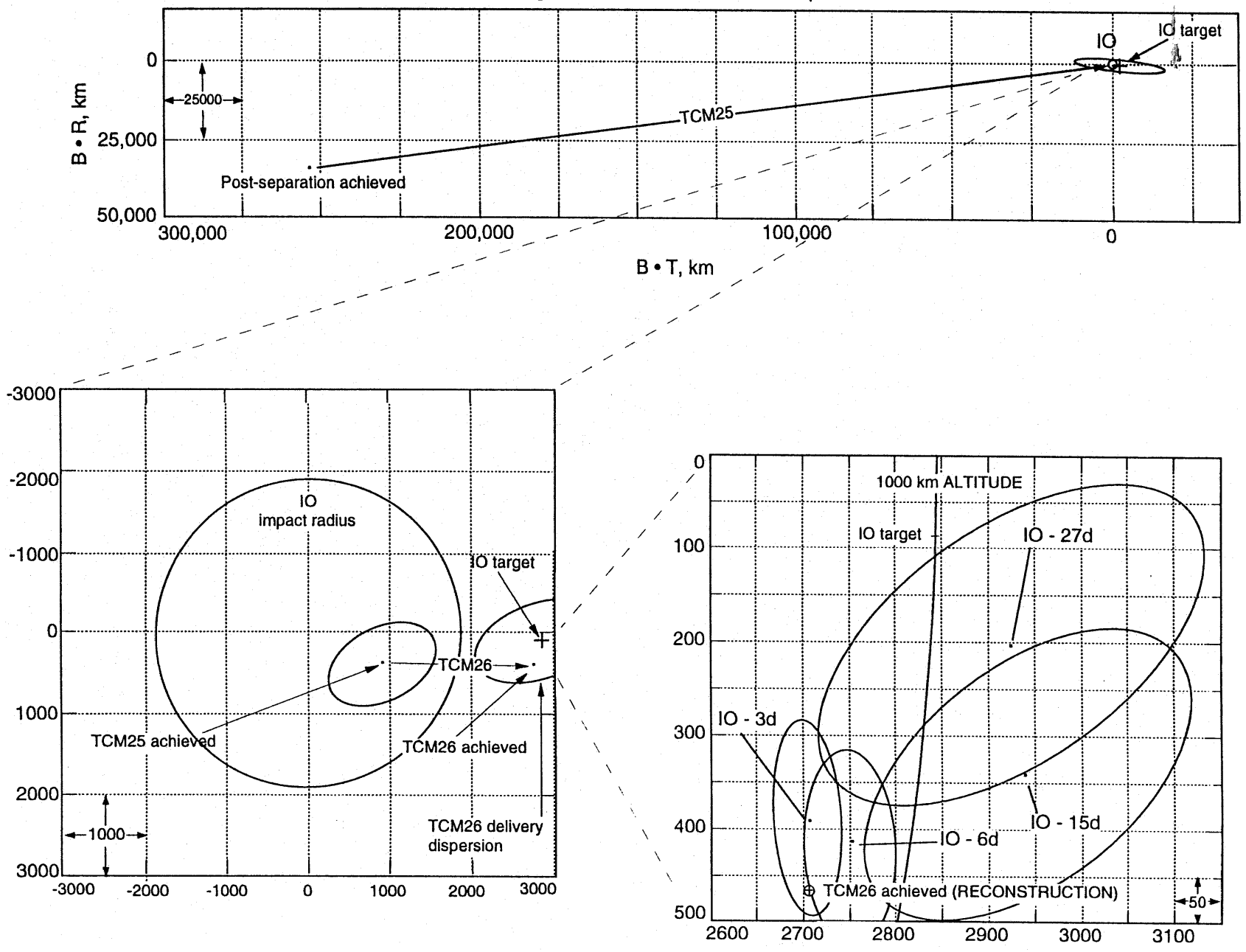

Fig 20

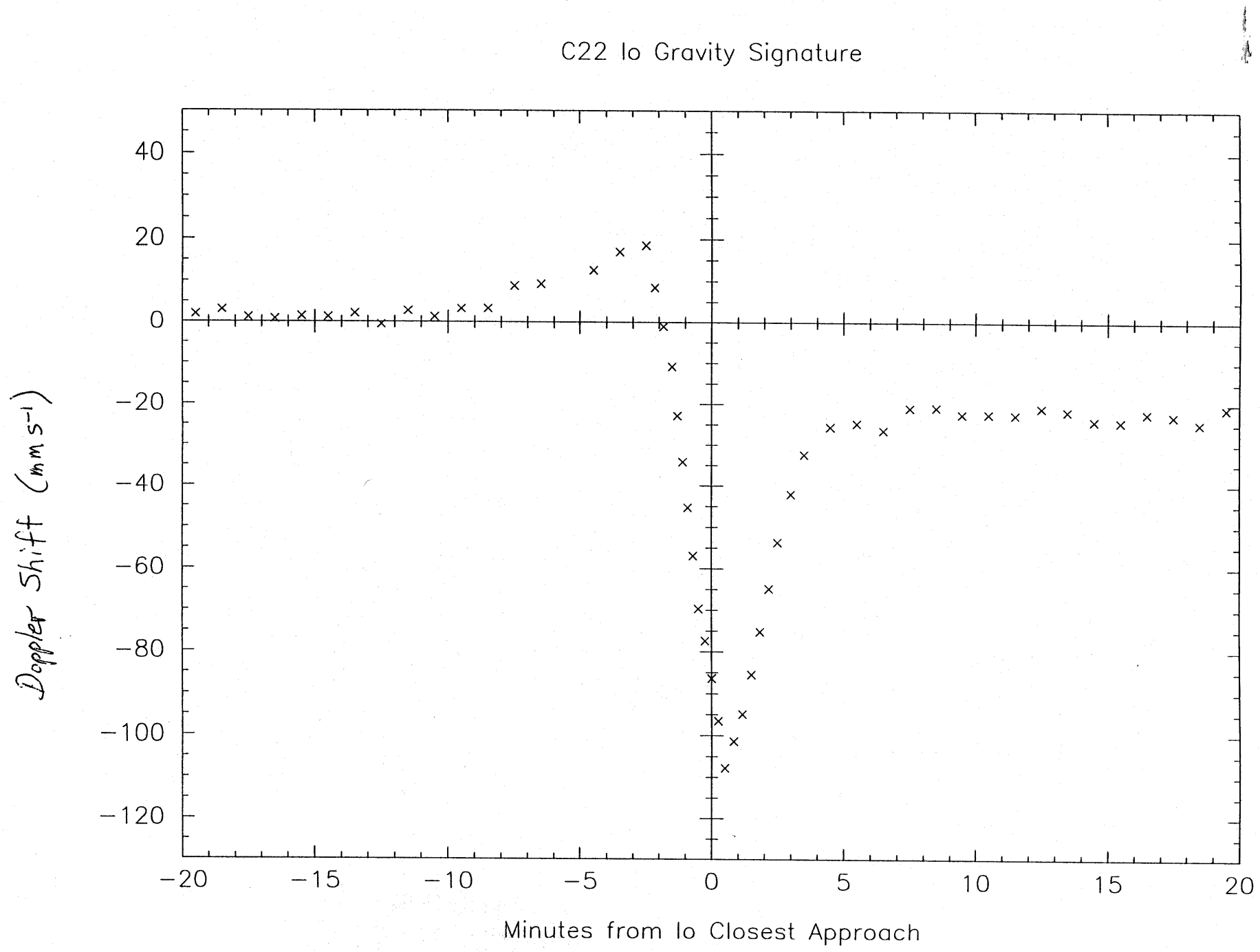
C22 Io Gravity Signature
40
20
0
−20
−40
−60
−80
−100
−120
−20
−15
−10
−5
0
5
10
15
20
Doppler Shift (mm s⁻¹)
Minutes from Io Closest Approach

Fig 21